BSc Thesis Biomedical Engineering

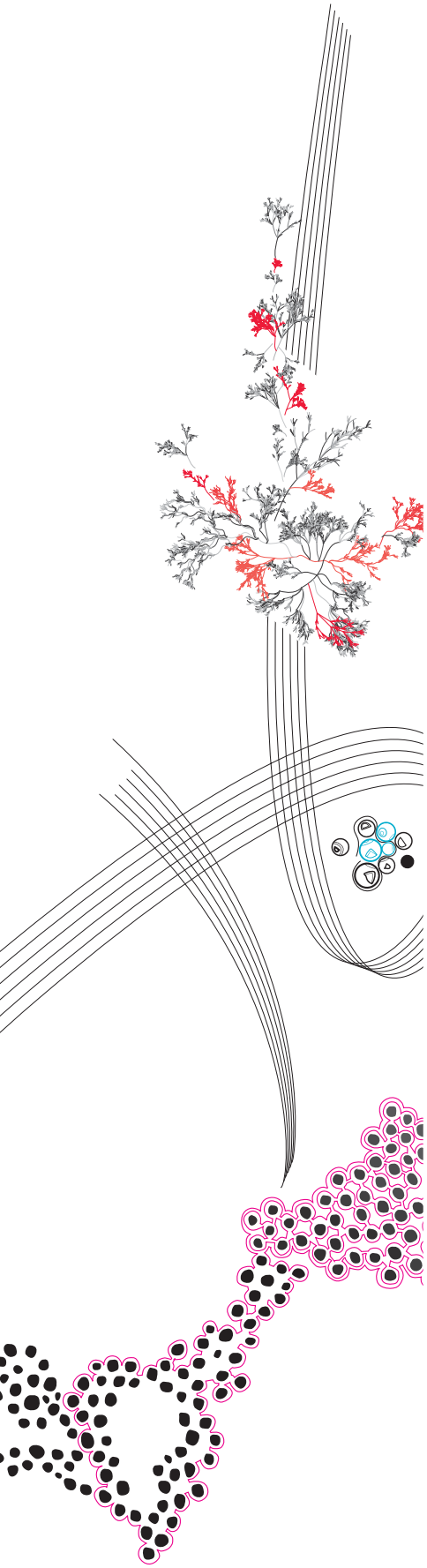

Quantitative spectroscopic photoacoustic imaging using reference fluence method

Youri H.W. Meevis

*S*2608073

Supervisors: F. Kalloor Joseph PhD *(BMPI)*

A. Thomas PhD *(BMPI)*

External supervisor: Dr. B. De Santi *(M3I)*

June 29, 2023

Department of Biomedical Photonic Imaging
Faculty of Science & Technology

UNIVERSITY OF TWENTE.

BMPI Biomedical Photonic Imaging

umcg

Abstract (NL)

De vorming van een atherosclerotische plaque in de halsslagaders kan de bloedtoevoer naar de hersenen verminderen en zelfs een beroerte veroorzaken. Dergelijke plaques kunnen onopgemerkt blijven en daarom is een niet-invasieve beeldvormingstechniek nodig om hun samenstelling en stabiliteit te bepalen. Fotoakoestische beeldvorming is een relatief nieuwe techniek die deze informatie kan verschaffen. Deze scriptie onderzocht of fotoakoestiek in staat is om het absorptiespectrum van een onbekende chromofoor (IRDye 800 CW) en de concentratie kwantitatief te bepalen. Dit wordt gedaan door gebruik te maken van een referentiechromofoor (Oost-Indische inkt), waarvan de absorptie bekend is, om te corrigeren voor de optische bestraling. Twee buizen, één met IRDye en één met Oost-Indische inkt, werden naast elkaar afgebeeld op drie verschillende dieptes ten opzicht van de transducer met in totaal drie verschillende concentraties van IRDye in het zichtbare nabij-infrarode spectrum. Het gecorrigeerde fotoakoustische signaal van IRDye 800 leek in zekere mate op het daadwerkelijke absorptiespectrum, maar met grote afwijkingen. Bovendien werd er geen duidelijke lineaire relatie gevonden tussen de beeldvormingsdiepte en de concentratie met het fotoakoustische signaal. De berekende concentratiewaarden lagen echter in dezelfde orde van grootte als de daadwerkelijke waarden. Dit betekent dat de compensatietechniek tot op zekere hoogte gerechtvaardigd is.

Abstract

Plaque formation in the carotid arteries can obstruct the blood flow to the brain and even induce a stroke. Such plaques can be unnoticed; therefore, a non-invasive imaging technique is needed to determine their composition and stability. Photoacoustic imaging is a relatively novel technique that may provide this information. This thesis investigated the possibility of photoacoustics (PA) to retrieve the absorption spectrum of an unknown chromophore (IRDye 800 CW) and its concentration quantitatively. This is done by using a reference chromophore (India Ink), which absorbance is known, to correct for the optical fluence. Two tubes, one with IRDye and one with India Ink, were imaged alongside each other at three different depths from the transducer with a total of three different concentrations of IRDye in the VIS-NIR spectrum. The compensated PA signal of IRDye 800 resembled the actual absorption spectrum to a certain extent but with major deviations. Furthermore, no proper linear relationship was found between the imaging depth and concentration with the PA signal. However, the calculated concentration values were in the same order of magnitude as the actual ones. This implies that the compensation technique is justifiable up to a point.

Contents

1 Introduction

Vascular diseases include a wide variety of death causations including ischaemic stroke which result in over 6 million deaths annually, making it the second-highest leading cause of death worldwide. [2] A stroke can be induced by a sudden rupture of a carotid artery plaque, an atherosclerotic lesion consisting of lipids, blood, collagen, cellular debris, etc., obstructing the blood flow in smaller vessels closer to the brain. See figure 1.1.
Before this occurs, however, the plaque may go unnoticed. The amount of carotid artery stenosis, narrowing, is currently investigated as a decision of intervention to prevent possible future strokes but this can lead to patient over-treatment [3]. Plaque composition, particularly lipid concentration and the vascular endothelia growth factor antibody (VEGF-A), are reliable predictors for plaque stability and thereby subsequent rupture. Unfortunately, no non-invasive imaging technique can provide this structural information yet. [4–6] Photoacoustic imaging (PAI) is a novel imaging modality that can perhaps overcome these boundaries and is therefore subject to much investigation in this thesis. [7]

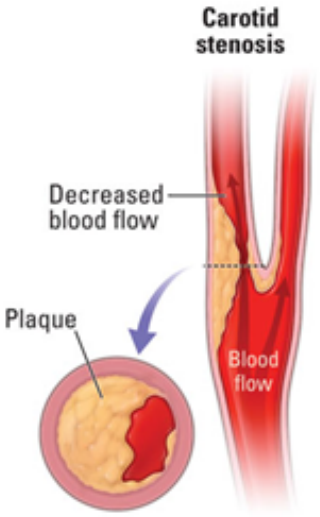

Figure 1.1: *A carotid plaque can cause stenosis of the artery resulting in a decreased or even complete obstruction of the blood flow. [1]*

1.1 Photoacoustic Imaging

Photoacoustics (PA) can be used to image soft tissues using the photoacoustic effect. True to its name, electromagnetic radiation is converted to sound waves due to thermoelastic expansion. Differences between optical and acoustic properties in different chromophores, light absorbing molecules, present in the tissue generate the image contrast. [8, 9]
The target tissue is illuminated with nanosecond pulses of laser light and the chromophores absorb this energy resulting in a small localised temperature rise. This leads to a pressure increase which subsequently relaxes resulting in a propagating wideband (MHz) acoustic wave which can be measured by one or more ultrasound transducers. When multiple A-lines are recorded and if the sound propagation speed in the sample is known, an image can be reconstructed via a multitude of different techniques such as backprojection via the inverse Fourier transform. [8] See figure 1.2

Photoacoustic imaging (PAI) combines the high penetration depth, approx. 4 mm, and spatial resolution, $< 100\ \mu$m, of ultrasonic sound waves and the high contrast sensitivity of optical imaging. The actual resolution, however, is still limited by the transducer center frequency, numerical aperture, and bandwidth. [10] Important to note is that spatial resolution decreases with increasing imaging depth. For vascular PAI, light mostly in the near-infrared (NIR) spectral region is used since it has a rather high optical penetration depth and the absorption spectra of lipids in that region differ from other biological components enhancing its image contrast. [7, 8, 11]

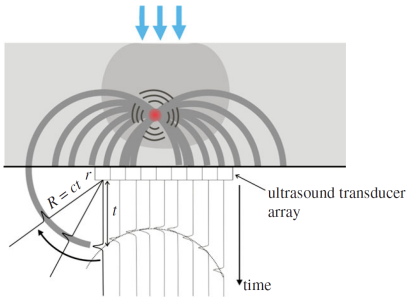

Figure 1.2: *A schematic overview of how the back-projection reconstruction technique with regard to photoacoustics works. [8]*

1.1.1 Quantitative PA spectroscopy

Inherently, PAI visualises the initial pressure distribution of optical energy conversion. As mentioned before, this is mostly due to the optical properties of the chromophores. Quantitative photoacoustic imaging (QPAI) uses the spectroscopic nature of the PA effect to quantify the chromophore concentrations via these properties. [9]

The initial pressure P_0 generated at point $\mathbf{r}$ of each optical wavelength λ is proportional to the absorbed optical energy $H(\mathbf{r}, \lambda)$ such that:

$$P_0(\mathbf{r}, \lambda) = \Gamma H(\mathbf{r}, \lambda) \tag{1}$$

Where Γ is the Grünheisen coefficient. A dimensionless constant that yields the efficiency of heat-to-pressure conversion. It is dependent on the volume of thermal expansivity, the speed of sound, and the heat capacity at constant pressure. [8] The wavelength-depended absorbed optical energy itself is given by the product of the absorption coefficient $\mu_a(\mathbf{r}, \lambda)$ and the light fluence $\Phi(\mathbf{r}, \lambda; \mu_a, \mu_s)$. Eq. 1 then becomes:

$$P_0(\mathbf{r}, \lambda) = \Gamma \mu_a(\mathbf{r}, \lambda) \Phi(\mathbf{r}, \lambda; \mu_a, \mu_s) \tag{2}$$

As one can see, the light fluence is dependent on both μ_a and the optical scattering coefficient μ_s. The contributions of these properties to the pressure signal, from now on referred to as the PA signal, is unknown since μ_a is also directly proportional to it. This makes Equ. 2 non-linear and as a result, Φ cannot be determined experimentally and must be modelled to quantify the PA signal, relating it back to the chromophore concentrations. [9]

Multiple numerical models of light propagation in tissue, such as the radiative transfer equation [12], Monte Carlo models [13] and parameter estimations [14] have been introduced in the past, but this research will follow a different approach. By assuming that the optical absorption, μ_a, contributes the most to the PA signal, then, in some specific cases, the relation between μ_a and the PA signal is linear and the influence of the change in light fluence, ϕ can be neglected. [9,15] This linear approach holds for when the signal is measured in a cylindrical object, such as a blood vessel or test tube, and its location should be exactly known, which can be obtained from ultrasound images. Additionally, μ_a of the blood should be known.

In this condition, the product of the absorption coefficient and the radius of the cylinder, a, should be significantly lower than 1: $\mu_a a \ll 1$. So this criterion mostly applies to very small blood vessels or tubes but a similar case also exists for larger radii. Then, the linear nature of ultrasound generation and propagation in biological tissues is used at high ultrasonic frequencies. The corresponding transducer center wavelength, Λ, will be much smaller than the cylinder radius such that $\Lambda \ll a$ and $\mu_a < 1/\Lambda$. Sivaramakrishan et al. [15] showed these relations experimentally and concluded there exists a linear and non-linear region in the function of normalised optical absorption ($\mu_a \Lambda$) and PA signal.

Huisman et al. [6] showed that the NIR optical tracer bevacizumab-800CW could visualise VEGF-A and was thereby able to determine carotid plaque stability. This was done using fluorescence imaging of angiogenesis in the plaques. This group conducted a subsequent research in which they studied the photoacoustic spectra of different concentrations of bevacizumab-800CW

in tubes with IRDye 800, a dye that has a characteristic peak in the NIR, as a reference. [5] They were able to retrieve the absorption spectra of both substances, albeit with minor differences, and found a correlation between the maximum PA signal and bevacizumab-800CW concentration. However, no significant quantitative analysis that took optical fluence into account was performed.

F. Kalloor Joseph from the Department of Biomedical Photonic Imaging at the University of Twente proposed the idea to use some sort of reference in a PA measurement to correct for the fluence. Here, the known absorption spectrum at a specific concentration of the reference is used. In a clinical setting, the artery blood surrounding the plaque could be used as this reference since its optical properties are known.

1.2 Research question and hypothesis

The main goal of this thesis is to investigate if it is possible to quantify the concentration of lipids within an *ex vivo* carotid artery plaque sample via QPAI using artery blood as a reference for the optical fluence. This will be investigated by using a known dye, with a known absorption spectrum, in a tube as a substitute for the plaque. The choice for this being IRDye 800 CW as it has a characteristic absorption peak around 775 nm, which can serve as a reference point, and Huismant et al. demonstrated that its absorption spectrum was retrievable via photoacoustics. [5] India Ink will be used as the reference for the optical fluence since it is widely available and its absorption spectrum is known.

To possibly quantify an unknown concentration of a substance via QPAI, it first needs to be investigated if QPAI is possible in doing just that. Cas Weernink looked into this query in his bachelor thesis *'Light fluence marker for quantitative photoacoustic imaging'*, conducting experiments with tubes containing India Ink. [16] He found that after applying multiple compensation methods, the absorption spectrum of India Ink derived from PA measurements resembled that of one measured with a spectrophotometer but was not exactly the same and hence, there was no proportional linear relation between μ_a and the PA signal found. [16]

This thesis will expand on Cas's research by conducting a similar experiment with IRDye 800 and determine if similar results can be achieved and built upon.

It is expected that the absorption spectrum of IRDye 800 is retrievable via PA measurements and it may or may not has some noise in its signal. It is not expected that a calculated concentration value will be exactly the same as the actual one but a difference should be measurable when experimenting with multiple concentrations.

2 Experiment overview

This chapter will explain the preparations, setup, measurement protocols, and data processing of the experiment.

Two tubes containing dilutions of substances are subject to QPAI. The test tube contains a concentration of IRDye 800 whereas the other tube, the reference, holds a known concentration of India Ink. A schematic of this is visible in figure 2.1. They were imaged, but most importantly, analysed to retrieve their absorption spectra and do determine the concentration of IRDye 800 in the test tube with only the PA signal. In total, three different experiments with test tubes, each with a different concentration of dye, were investigated. One test tube per measurement.

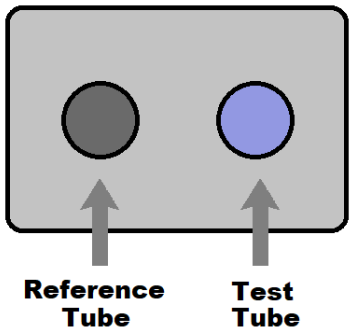

Figure 2.1: *A schematic representation of the experiment in which two tubes, the reference, and the test, are situated next to each other and imaged via PA. Please note that neither the transducer nor the laser is included in the image.*

The experiment was performed with an MSOT Acuity Echo prototype (iThera Medical GmbH, Oberschleißheim, Germany) situated at the Department of Nuclear Medicine and Molecular Imaging at the University Medical Center Groningen (UMCG), the Netherlands. This device can be used for clinical ends as it can scan through a spectral region and show the live footage of multiple wavelengths in, addition to the ultrasound signal, to the user. These advantages make it possible to conduct many measurements in a relatively short amount of time.

2.1 Preparing the dilutions

For the experiment to give proper results, the value of the absorption coefficient of the dilutions should resemble the one of artery blood. At $\lambda = 800$ nm, μ_a of artery blood is 0.38 mm^{-1}. [17] Therefore, the μ_a of the India Ink reference should have the same value. Furthermore, the criteria introduced in Section 1.1.1 should be accounted for. [15] The transducer that is used has a center frequency of 4 MHz corresponding to an acoustic wavelength (Λ) of 0.317 mm, assuming a sound propagation speed of 1485 m/s. At $\mu_a = 0.38$ mm^{-1}, those criteria will be satisfied for a linear PA signal response since $1/0.371 = 2.70$ mm^{-1} is larger than 0.38 mm^{-1} and the radii of the tubes are significantly larger than 0.31 mm.

Assuming uniform concentration, and thereby uniform attenuation of the substance across the whole tube, the molar absorption coefficient of a substance can be derived via equations from the Beer-Lambert law:

$$A = log(\frac{I}{I_0}) = \epsilon cl$$
$$\frac{\mu_a}{ln(10)} = \epsilon c \tag{3}$$

With A being the absorbance (a.u.), I and I_0 the intensity of the incident and measured light respectively, ϵ the molar extension coefficient, c the molar concentration and l the optical path length. If ϵ is known, this equation makes it possible to calculate the concentration of a substance with a known absorption coefficient and vice versa. Eq. 3 can also be rewritten as:

$$\mu_a = \frac{ln(10^A)}{l} \tag{4}$$

Since l is equal to the length of the cuvette, 10 mm, μ_a is only dependent on the absorbance and more specifically, the measured intensity I_0 for a specific wavelength, in this case 800 nm.

2.1.1 Correcting for the fluence using the reference tube

As mentioned in Section 1.1.1, a reference sample is used to correct for the fluence. Here, the same method is used as in Cas's thesis [16]. The absorbance of India Ink at a specific concentration is measured with a spectrometer and the corresponding μ_a is calculated for each wavelength. After the PA signal of the reference tube for each wavelength has been obtained, the spectrometer data divides by it. The resulting value is a scalar: Eq. 5. Then, the PA signal value of the test tube is multiplied by that scalar for each wavelength as shown in Eq. 6. Now, the photoacoustic IRDye 800 measurements are compensated for the fluence.

$$C_\lambda = \frac{Spec.\ \mu_{a\ (India\ Ink,\lambda)}}{PA\ signal_{(ref,\lambda)}} \tag{5}$$

$$PA\ signal_{(compoensated,\lambda)} = PA\ signal_{(uncompensated,\lambda)} \cdot C_\lambda \tag{6}$$

This compensation method assumes that all the external factors inside and between the tubes remain the same during the measuring time.

2.1.2 Test: IRDye 800 CW

5 mL of three different dilutions of IRDye 800 CW (LI-COR, Lincoln, NA, USA) have been made with a μ_a resembling that of artery blood at 800 nm, corresponding to a value of 0.38 mm^{-1}. After the absorbance has been measured by a spectrophotometer (Shimadzu UV-2600/2700, Kyoto, Japan), the corresponding concentrations were calculated by using Eq. 3 since the molar extinction coefficient of the dye is known: 24,200 $M^{-1}mm^{-1}$. A stock dilution was made first from a master stock (ca. 4.3 mM in DMSO) available at the UMCG. 50 μL of this master stock was diluted with ca. 4.2 mL of Milli-Q water to achieve a new stock dilution of 50 μM. From this new stock, the three test dilutions have been made by adding a certain amount to a test tube and filling it up to 5 mL with Milli-Q water. The specific amounts for each dilution can be seen in Table 1 along with their respective concentration and absorption coefficient values.

Table 1: *The absorption coefficients, corresponding concentrations, and constitutes of the IRDye 800 dilutions being measured with PA.*

Absorption coefficient IRDye 800 (mm^{-1}) at $\lambda = 800$ nm	Corresponding concentration IRDye 800 (μM)	Corresponding amount of IRDye 800 (μL) : Milli-Q water (μL)
0.38	6.82	682 : 4318
0.48	8.61	861 : 4139
0.58	10.41	1041 : 3959

The retrieved absorption spectra via photoacoustic should be compared with a 'ground truth'. Therefore, the absorption of the dilutions was first measured with a spectrophotometer in the same spectral range as the MSOT device. However, according to the manufacturer, the used spectrophotometer does not give trustworthy results when the measured absorption is higher than 2 units. When using Eq. 3, this value gets surpassed for concentrations of approx. 8.61 μM and higher. Therefore, the choice has been made to measure with lower concentrations to ensure trustworthy results and then extrapolate the absorbance values so that they correspond to the concentrations that are being used for the PA measurements. It must be noted that this approximation of absorbance values only holds when the relationship between absorbance and concentration is linear. The measured and extrapolated absorption spectra of all these concentrations can be seen in figure 2.2 and an overview of the absorbance values of the measured ones and calculated μ_a at 800 nm in Table 2.

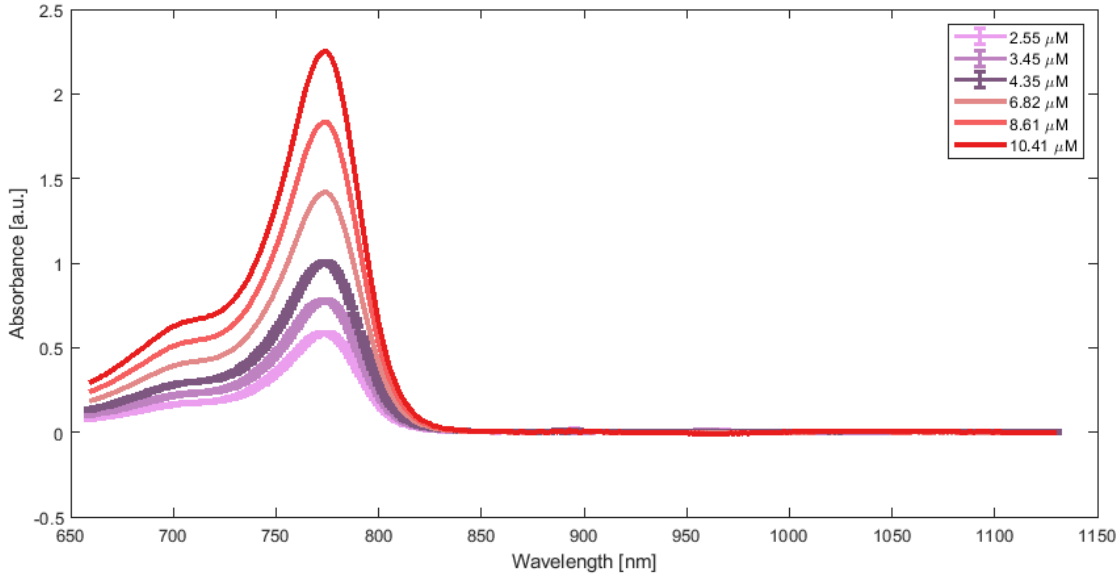

Figure 2.2: *The measured absorption spectra of three concentrations of IRDye 800 CW via a spectrophotometer (purple) and the extrapolated spectra corresponding to the concentrations used in the PA measurements (red). The average values of the measured values consist of two measurements with a 24-hour time difference between them. The characteristic peak at around 775 nm is clearly visible for all three concentrations in addition to the plateauing at 700 nm. Furthermore, after approx. 830 nm, there is no absorbance for any concentration.*

Table 2: *The absorbance and corresponding calculated μ_a of three different dilutions measured at λ = 800 nm.*

Dilution (μM)	Measured absorbance (a.u.) at λ = 800 nm	Calculated μ_a (mm^{-1}) at λ = 800 nm
2.55	0.1695 ± 0.0021	0.0389 ± 0.0006
3.45	0.2255 ± 0.0064	0.0518 ± 0.0016
4.35	0.2890 ± 0.0057	0.0664 ± 0.0015

2.1.3 Reference: India Ink

One dilution of India Ink (Royal Talens bv, Apeldoorn, the Netherlands) with the same $\mu_{a,\lambda=800}$ (0.38 mm^{-1}) has also been made to serve as the reference. However, the concentration of the used stock dilution is unknown so the corresponding concentration of the desired μ_a had to be determined experimentally. This was done by making 50 mL of three arbitrary dilution ratios first, then measuring their absorbance at 800 nm, calculating the corresponding μ_a, and then making a linear fit through those measurements. With this, the dilution ratio of a desired $\mu_{a,\lambda=800}$ could easily be derived. The constituents of the ratios can be found in Table 3 and figure 2.4 shows the linear fit through the measurement absorption points at 800 nm. Figure 2.3 shows the absorption spectrum of India Ink of a concentration of $\mu_{a,\lambda=800}$ = (0.38 mm^{-1}).

Table 3: *The constituents of the three arbitrary India Ink dilution ratios that have been used to make the linear fit with.*

Dilution ratio India Ink : Milli-Q water	Amount of India Ink (μL) : Milli-Q water (mL)
1 : 4000	12.5 : 50
1 : 2000	25.0 : 50
1 : 1500	33.5 : 50

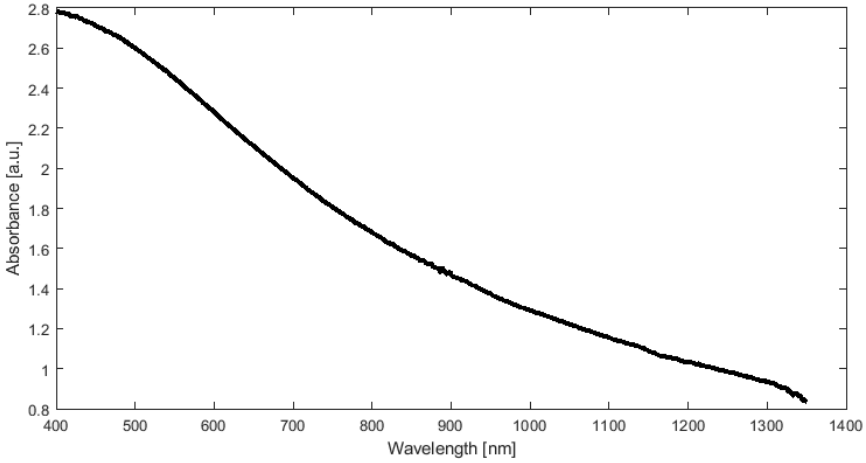

Figure 2.3: *The absorption spectra, measured via a spectrophotometer, of India Ink with a concentration of μ_a = 0.38 mm^{-1} at 800 nm.*

It was found that for $\mu_{a,\lambda=800}$ = 0.38 mm^{-1}, the dilution ratio should be approximately 1:1706. Three dilutions were made by adding 29.3 μL India Ink in 50 mL Milli-Q water. To ensure that the right dilution were made, $\mu_{a,\lambda=800}$ was determined again: 0.38683 ± 0.00227 mm^{-1}. However, previous PA measurements showed that an India Ink dilution of $\mu_{a,\lambda=800}$ = 0.38 mm^{-1} had a relatively low PA signal. To ensure that the PA signal from the reference

tube is sufficient in all conditions, the choice has been made to increase the concentration to a value of $\mu_{a,\lambda=800} = 0.59$ mm^{-1}. This value lies in the upper range of the error of $\mu_{a,\lambda=800}$ values of artery blood. [18] The corresponding dilution is ca. 1:1087 (or 46.0 μL India Ink in 50 mL Milli-Q water). However, this was calculated with the same linear fit that was made with lower concentrations. So this was an extrapolation which may be more sensitive to errors. Two dilutions have been made: 0.59314 ± 0.00898 mm^{-1}. Both new dilutions can also be seen in figure 2.4 as orange points.

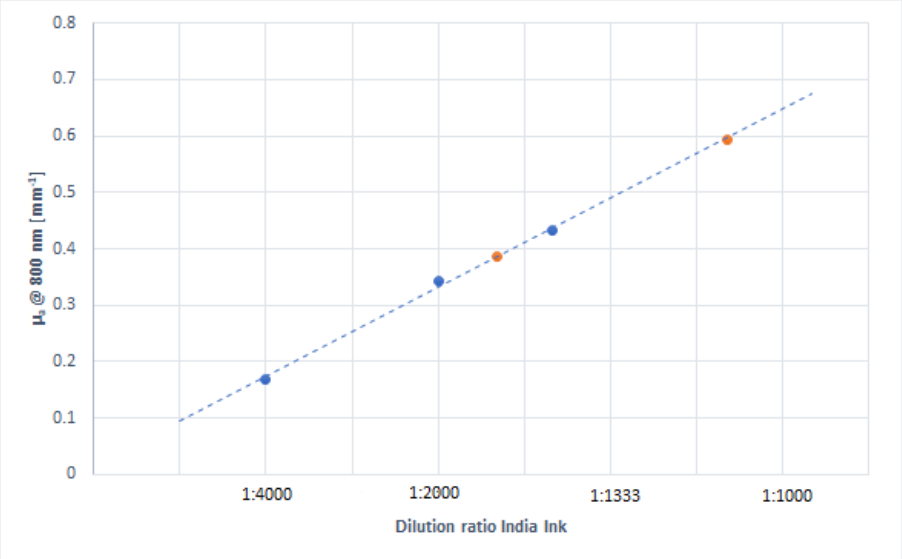

Figure 2.4: *The linear fit through the measured $\mu_{a,\lambda=800}$ of the three India Ink dilutions (blue) and the calculated 0.38 and 0.59 mm^{-1} dilutions (orange). The corresponding equation of the fit is: 'y = 0.1571x + 0.0117' where x is the dilution ratio normalised to 1:4000 and y is $\mu_{a,\lambda=800}$. For y = 0.38 and 0.59, x = 2.34 and x = 3.68 corresponding to a dilution ratio of 1:1706 and 1:1087 respectively*

2.2 Requirements and experimental set up

Now, an overview of all the required materials for the experiment is presented and discussed.

- The iThera Medical MSOT Acuity Echo prototype
- Measuring probe connected to the device with a build in:
  - 2D concave transducer detector (4-MHz center frequency, 256 transducer elements, spatial res.: approx. 180 μm)
  - 25 Hz pulsed nd: YAG laser (660-1300 nm; 25 mJ pulses)
- Custom designed 3D-printed tube and probe holder
- Filled water tank (approx. 9-10 L total)
- India Ink to mimic optical absorption of soft tissue
- Intralipid (20%) to mimic optical scattering of soft tissue
- Two tubes containing the reference (India Ink) and test substances (IRDye 800) respectively

To accurately mimic the absorption and scattering properties of soft tissue, India Ink and intralipid are added to the water respectively. For soft tissue, approx. $\mu_{a,\lambda=800} = 0.005$ mm^{-1} [19]. The corresponding dilution of India Ink has been calculated with the same linear fit in figure 2.4 and was determined at 1:166,667 or 6 μL India ink per 1 L of water. Initially, intralipid would be used to mimic the scattering properties of soft tissue. However, on the day that the experiment was conducted, no intralipid was available so an alternative had to be found on short notice. The choice was made to use (biological) whole milk (Arla Foods, Nijkerk, the Netherlands) as previous studies have shown that it could also be used as a scattering medium for photoacoustic experiments and it is widely available. [20, 21] However, the exact scattering properties of whole milk are unknown so that had to be determined afterwards with the inverse adding-doubling method [22]. The method for this is presented in Section 3.2

The tubes were placed into a specialised 3D-printed holder that is attached to the transducer probe so the distance between the tubes and the transducer did not change during a measurement. The holder was designed in such a way that the tubes could be placed at many different depths from the transducer and at different distances from each other. During the experiment, it was noted that the most upper row of holes could not have been used since the lower part of the transducer overlapped there. The 3D model can be seen in figure 2.5.

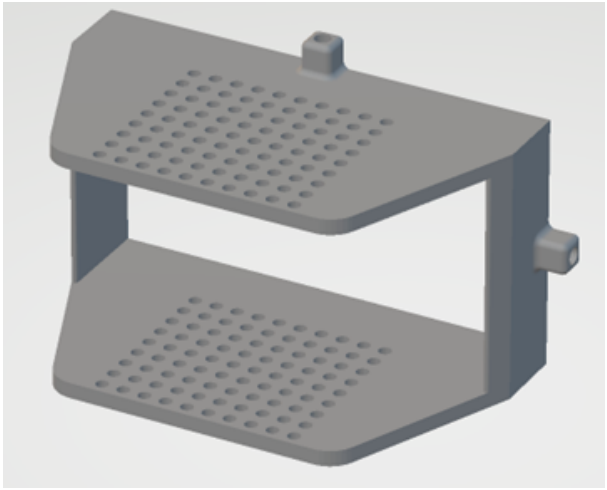

Figure 2.5: *A 3D render of the custom-designed probe and tube holder. The spacing between the holes is 7 mm (center to center) and the distance between the lower part of the transducer and the second row of holes is 3 mm.*

It is important that the interference of the tubes to the PA signal should be limited to a minimum. Therefore, multiple different tubes should be characterised to determine the most optimal tube material. It must be noted that this characterisation has not been conducted with the MSOT Acuity Echo at the UMCG, but with a self-build experiment configuration at the Department of Biomedical Photonic Imaging at the University of Twente, the Netherlands. Cas has used this configuration for his bachelor thesis so a detailed overview of the configuration and protocols can be found there. [16] The tube, situated at the focus of the transducer, was taped to a metal component, and black insulation tape was placed close to it next to it to localise it via the live footage. After the location of the tube and tape were determined, the tape was removed and the resulting signal, of only the tube, was determined. How larger the standard noise pattern of the PA signal, with a corresponding smaller average intensity value, how smaller the tube interference signal. This was done twice, with an empty tube and one filled with an

India Ink concentration. Everything was determined qualitatively. The following tubes were characterised:

1. Silicone - 2 mm inner - 4 mm outer diameter (Instech Laboatories Inc., Plymouth Meeting, PA, USA)
2. Silicone - 4 mm inner - 6 mm outer diameter
3. Silicone - 3 mm inner - 5 mm outer diameter (Lettix bv, Apeldoorn, the Netherlands)

Tube 3 showed the least amount of interference in the reconstructed image and was therefore used to conduct the experiments with.

Figure 2.6: *Pictures depicting the experiment configuration with a filled water bin (left) and an empty bin (right) to visualise the tubes with regard to the holder and transducer positions.*

2.3 Measurement Protocols

The MSOT Acuity Echo is designed for clinical use and therefore, data acquisition is rather straightforward since a physician must be able to work with it without too much effort to ensure the comfort of the patient. A scan can be seen as a video in which it 'sweeps' through the whole spectrum resulting in one frame per measured wavelength. When it has reached the end of the spectrum, it will start again from the beginning resulting in another sweep. How longer a measurement last, the more sweeps are collected. As mentioned before, three different IRDye 800 concentrations, Table 1, were measured at three different depths: 3 mm, 10 mm, and 17 mm. Each condition was measured *in triplo* resulting in 27 scans in total. Furthermore, to characterise the scattering properties of whole milk, another series of scans were made where the concentration of milk was steadily increased until the IRDye 800 signal was no longer visible on the live footage (680 nm) while measuring the tubes at 10 mm depth. Detailed protocols for taking these measurements can be found in appendix A.1. The scans of multiple different concentrations of whole milk were used to quantify the scattering properties of it using the inverse adding doubling method. More information regarding this can be found in Section 3.2.

2.4 Data processing

After all the scans have been collected as .msot files, each of them was converted to a .mat file so Matlab was able to read the data. The Python script, `MSOT_to_MAT_converter.py`, that was used for this can be found in appendix A.3. Other parameters, other than the sinograms,

that have been saved by this script were the laser pulse energies at each wavelength of each sweep, and the sensor position and the number of sweeps for each wavelength.

A Matlab script `PA_DASReconstruction_and_ROIs_collection.m` was used to reconstruct the image and collect the PA-signal data from both tubes of each scan. This script can be found in appendix A.4. Each sinogram gets normalised and corrected for the corresponding pulse energy value by dividing by the value itself. Then an average sinogram of all the sweeps is made to reduce the noise. This sinogram then gets filtered through a band-pass (cutoff frequencies: 2 and 6 MHz) and reconstructed using the 'Delay and Sum' method using a speed of sound of 1480 m/s. Two circular regions of interest (ROI) corresponding to the tube locations are made. See figure 2.7. The pixels which intensity values (PA signal values) higher than half of the maximum value inside one ROI are selected and one average is made of them. It is assumed that these values correspond to the signal of the substance inside the tube. Since a circular ROI only depicts one cross-section of a tube, it is assumed the measured values represent the whole inside of the tube. The script saves a table with the average PA signal value of the reference and test tube corresponding to each wavelength.

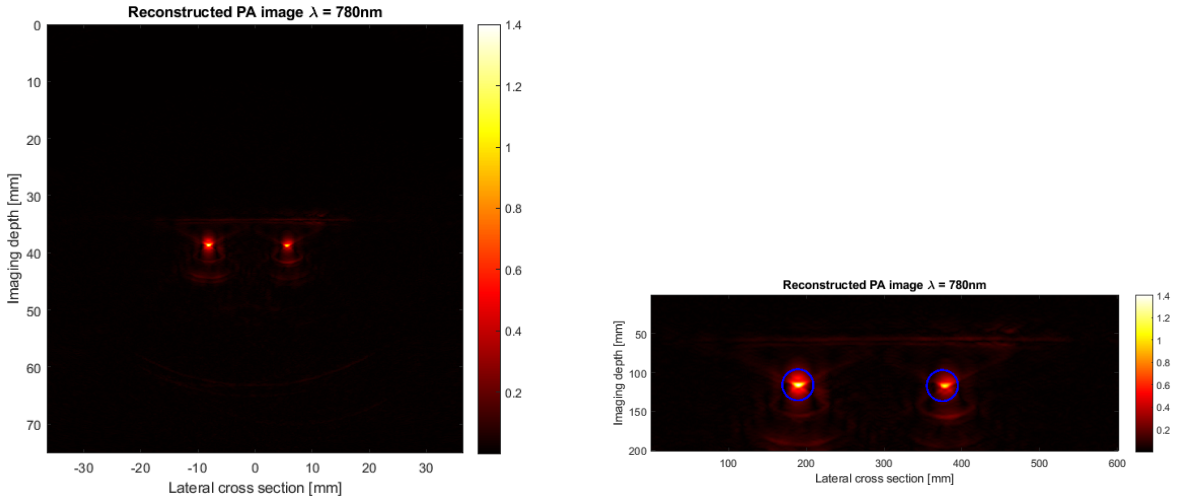

Figure 2.7: *A reconstructed PA image using the 'Delay and Sum' method (λ = 780 nm (average of all sweeps), concentration = 10.41 μM, imaging depth = 3 mm). The left figure shows the whole reconstructed image and the right one is zoomed in on the two tube signals in which the blue circular ROI edges have been plotted. The image let it seem like the signals are at 40 mm depth. However, the y-axis is not corrected for the transducer placement. In reality, the tubes are situated 3 mm from the transducer. An artifact from the transducer is visible in the image as a horizontal line above the ROIs. Please note that the axis in the left figure does in fact not correspond to mm but the pixel number as those were easier to work with when determining the ROI locations.*

Another Matlab script, `PA_ROIs_analysis.m` visible in appendix A.5, collects the measured spectrophotometer absorption data of India Ink ($\mu_{a,\lambda=800} = 0.59$ mm^{-1}). These values first get converted to absorption coefficient values, μ_a, using Eq. 4. Then, they get divided by the PA signal values of the reference tube, saved in the table of the previous script, to get a correction scalar at each wavelength; Eq. 5. This correction is then applied to the test tube data, by multiplying with it, to correct for the fluence. See Eq. 6. Thus, for each condition, there is a specified correction scalar for each wavelength.

3 Data analysis

In this chapter, all data from the measurements are analysed and presented in such a way that multiple graphs could be plotted in which relations of different parameters of interest, such as IRDye 800 concentration and imaging depth, with the PA signal, become visible. Eventually, the actual concentration of IRDye 800 with the calculated concentration from PA measurements is compared to each other to determine if QPAI is capable of determining the concentration of a chromophore.

3.1 Laser energy and the number of pixels in the ROIs

First, it must be noted that the laser pulse energy differs per wavelength, and even per sweep number. Figure 3.1 shows this energy variation over the measured spectrum.

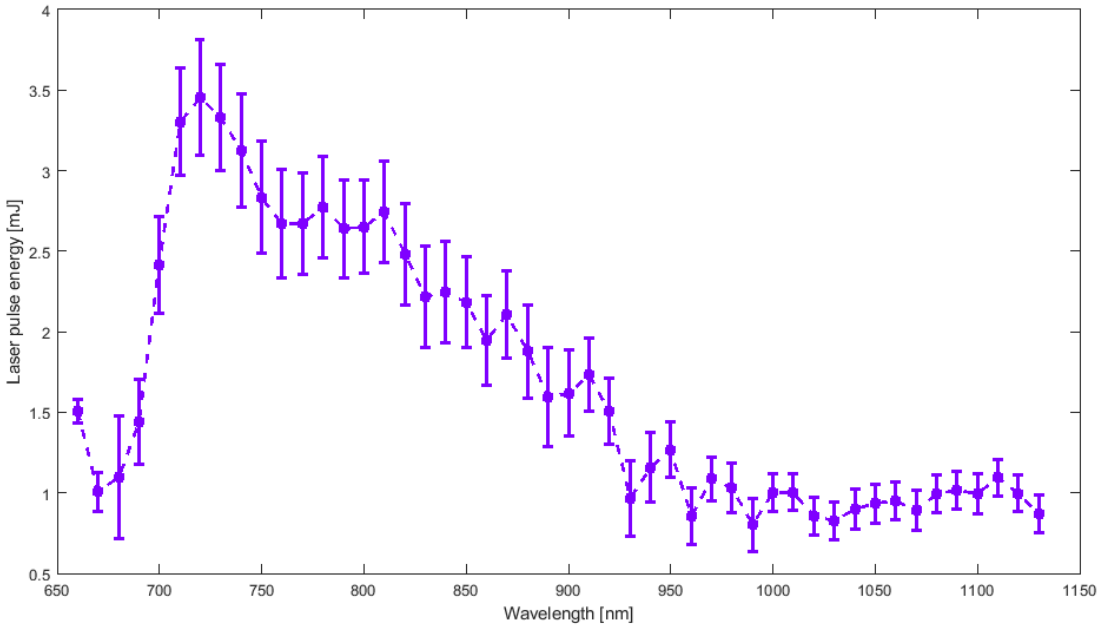

Figure 3.1: *The laser pulse energy for each wavelength of all the scans. The values contain all the energy values at each sweep in one average.*

As one can see, the difference in pulse energy widely varies across the measured spectrum; from almost 0.8 to 3.5 mJ. Therefore, each sinogram was corrected for this by dividing it by its corresponding laser energy value as mentioned in Section 2.4. The energy values start out low, but highly increase peaking at 720 nm after which it declines steadily. After approximately 900 nm, the energy is significantly lower than in the 700 to 850 nm region. As a result, the compensation in that spectral region has less influence on the sinograms. Even so, when the laser energy is lower than 1.0 mJ, all the pixel intensity values in those sinograms get larger, including the ones consisting of only background noise. This could result in incorrect tube signal values in that region.

Furthermore, not all pixels present in the circular ROIs are being used to calculate the average tube signal with; only the pixels whose intensity values are half of the maximum value in the corresponding ROI and higher. This results in the fact that not the same amount of pixels get used for each ROI average. Figure 3.2 shows a graph in which the number of pixels used in

the average ROI value calculation is plotted against the wavelength.

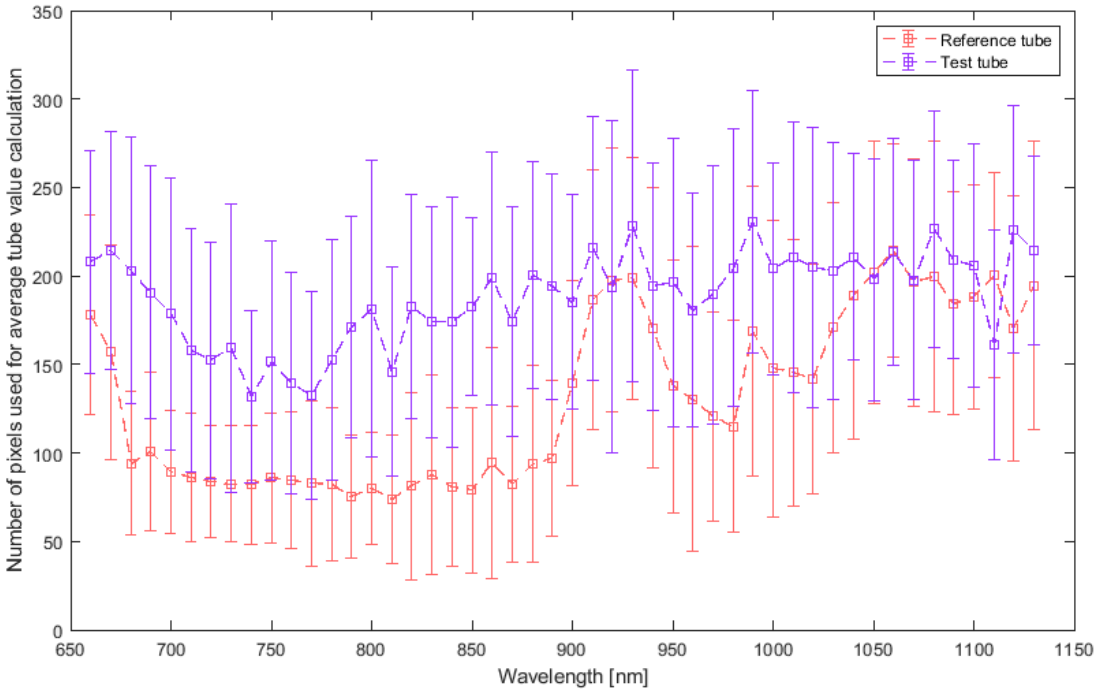

Figure 3.2: *The number of pixels in the ROI used to calculate the average PA signal of the corresponding tube plotted for each wavelength.*

As one can see, more pixels get used for averaging in the ROI corresponding to the test tube than the one of the reference tube. This can be explained by the fact that the PA signal in the reference tube is higher than in the test tube. The maximum pixel intensity value in the ROI of the test tube will therefore be closer to the lower pixel intensity values corresponding to noise. As a result, more pixels in that ROI are higher than half of the maximum value compared to the ROI of the reference tube. Nevertheless, both ROIs show a rather large standard deviation in the number of pixels. However, the standard deviation is smaller where the laser energy is higher and where the IRDye 800 has significant absorption (approx. 700 - 800 nm). In other words, the number of pixels that are averaged is somewhat constant, and a comparatively lower standard deviation is found if there is a high-contrast reconstruction image of targets. In this case: the tubes.

3.2 Scattering properties of whole milk.

The inverse adding doubling method was used to determine the scattering properties of the whole milk used as the scattering medium mimicking soft tissue. Here, a Matlab model was used to determine the reduced scattering and absorption coefficients of a sample in a spectral region of interest [22]. The samples of interest are whole milk samples at different concentrations that were used in the second batch of measurements as described in Section 2.3. A 2 mm thick polystyrene sheet was used as a reference sample since the absorption and reduced scattering coefficient values of that material were known at 600 and 800 nm. The transmittance and reflection of this reference sheet were measured at each wavelength in our spectral region of interest

(660 to 1130). With this, the reduced scattering and absorption spectrum was calculated via the model and fitted to our spectral region of interest. These are presented in figure 3.3. Now that the appropriate parameters of the model have been set, the transmittance and reflection measurements of the milk samples were planned to be inserted into the model to receive their scattering and absorption spectrum. However, because of the large difference between the optical properties of the polystyrene sheet and the whole milk samples, the model was unable to determine this and failed to provide adequate results. Due to this obstacle and time constraints, it was not possible to determine the scattering properties of whole milk.

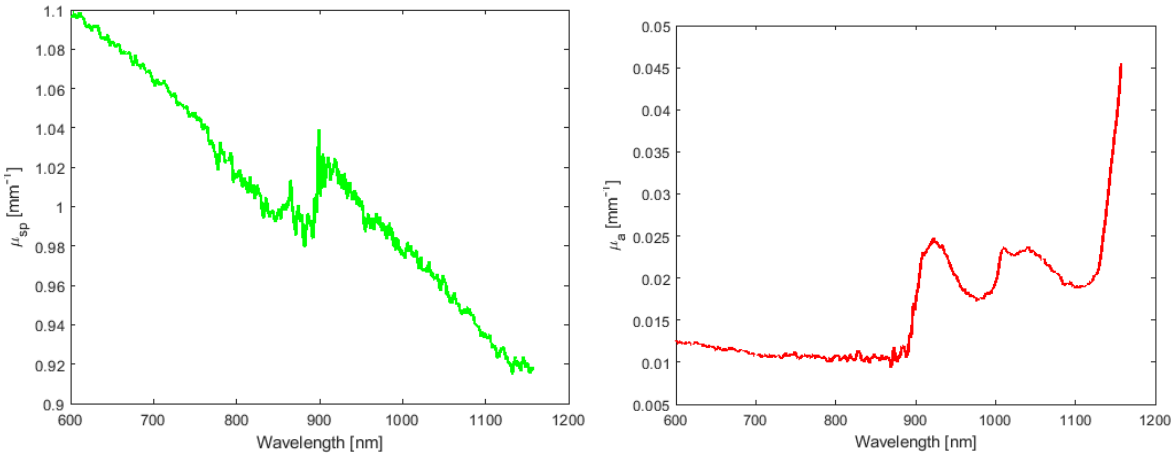

Figure 3.3: *The reduced scattering (left) and absorption coefficient (right) of a 2 mm thick polystyrene reference sheet was used to determine the scattering properties of whole milk. The reduced scattering spectrum seems to linearly decrease but a sudden leap can be seen at around 900 nm. This can be explained by the fact that the spectrometer uses two detectors to measure the light intensity, one for below 900 nm and one for above. At this point in the spectral region of interest, the detector needs to be switched. Sometimes, this does not occur correctly and a deviation between the measured intensity is found. This error is, however, not found in the absorption spectrum which implies that this has something to do with measuring the reflection inside of the spectrophotometer.*

To present some results with respect to the milk scattering nonetheless, a quick search in literature has been done. Aernouts et al. determined the absorption and reduced scattering spectra of 60 raw milk samples from different cows using the inverse adding doubling method. [23] For a 27 mL sample with a fat percentage of 3.38 % (the lowest concentration used), the measured reduced scattering coefficient was 1.8 mm^{-1}. A few notes must be made. First, the raw milk they used was unpasteurised and not diluted. The fat percentage was determined experimentally beforehand (ISO 9622; ISO, 2000). In short, this does not resemble the properties of the milk used in this thesis, as that fat percentage is unknown, it was pasteurised and diluted with water. The percentage of milk in water that was used in this experiment was 0.552 % and the percentage of total fat inside is therefore even lower. Due to all these differences, it is assumed that no adequate approximations can be constructed using this paper with regard to the milk used in this thesis and is therefore not further investigated.

3.3 The fluence compensation using the India Ink reference tube

The compensation method presented in Eq. 5 & 6 to retrieve the absorption spectrum of IRDye 800 is now highlighted. Figure 3.4 shows the India Ink absorption spectrum, $\mu_{a,\lambda=800} = 0.59$ mm^{-1}, measured by the spectrophotometer (absorbance unit = blue plot, μ_a = orange plot) and the MSOT device (yellow plot, concentration IRDye 800 = 10.41 and 6.82 μM, depth = 3

mm and 10 mm upper and lower figures respectively). The compensations scalar values are the orange plot divided by the yellow plot.

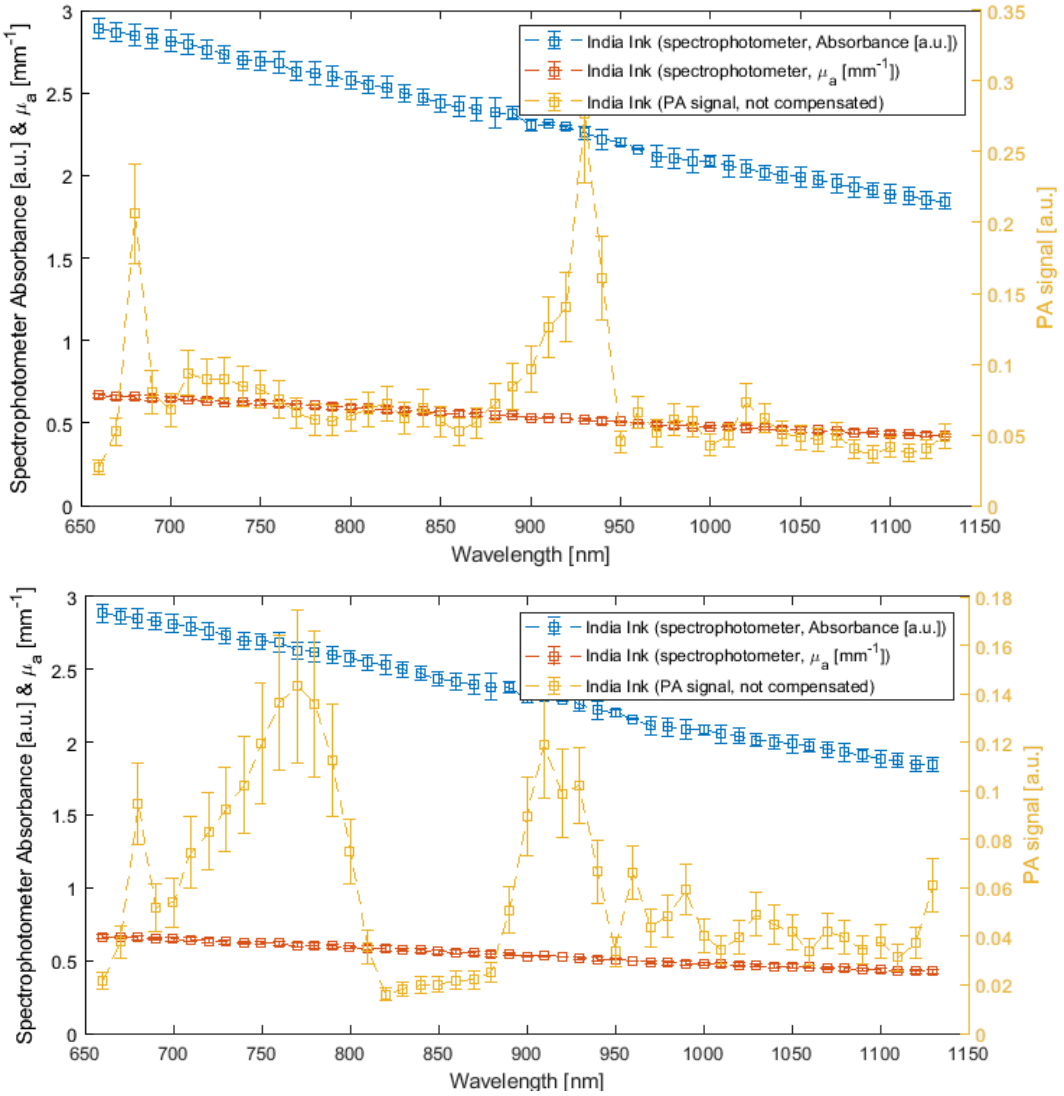

Figure 3.4: *Three different plots of the absorbance of India Ink with concentration $\mu_{a,\lambda=800} = 0.59$ mm^{-1}: Blue = Absorbance unit measured by the spectrophotometer, orange = calculated μ_a from the absorbance and yellow = PA signal (proportional to the absorbance) from the MSOT device (concentration IRDye 800 = 10.41 and 6.82 μM, depth = 3 and 10 mm upper and lower figures respectively). The correction scalar to multiply the test tube PA signal with is calculated by dividing the orange plot by the yellow plot. Please note the two different y-axes.*

The outline of the PA signal plot is clearly different than the ones of the spectrophotometer. For instance, there are two significant peaks at 670 and 930 nm and the signal itself is more 'noisy'. However, the lower absorbance at higher wavelengths is still somewhat visible at an imaging depth of 3 mm. Similar results have been found for other concentrations of IRDye 800 and at an imaging depth of 17 mm. The peaks do not correspond to other noteworthy values in the laser energy and number of pixels in ROI plots thus there is no causation to be found in that regard. Therefore, it is assumed that these outliers are characteristic of the PA measurements. Furthermore, when looked at the same graph but for an imaging depth of 10 mm and a concentration of 6.82 μM specifically; an unexpected increase of the PA signal is

found from 700 nm in which it decreases rapidly to almost plateauing at 800. This is highly unexpected behaviour that was not found in other depths and concentrations. Therefore, this outlier is regarded as an error in conducting the measurements. This error may have an influence on further analysis of the results.

3.4 The absorption spectrum of IRDye 800 CW.

Now, the absorption spectrum of IRDye 800 CW can be retrieved. Nine different spectra can be formed, one for each condition. Figure 3.5 depicts the one for a concentration of 6.82 μM at 3 mm imaging depth as it showed the characteristic absorption peak around 775 nm the most clearly. Three different plots are made: the PA signal derived from the ROI that has been compensated for the laser energy but not for the fluence, the same signal that is compensated for the fluence, and a Fourier fit (8th degree) of that last plot. A Fourier fit was chosen since it followed the overall shape of the plot better than a polyfit of the same degree.

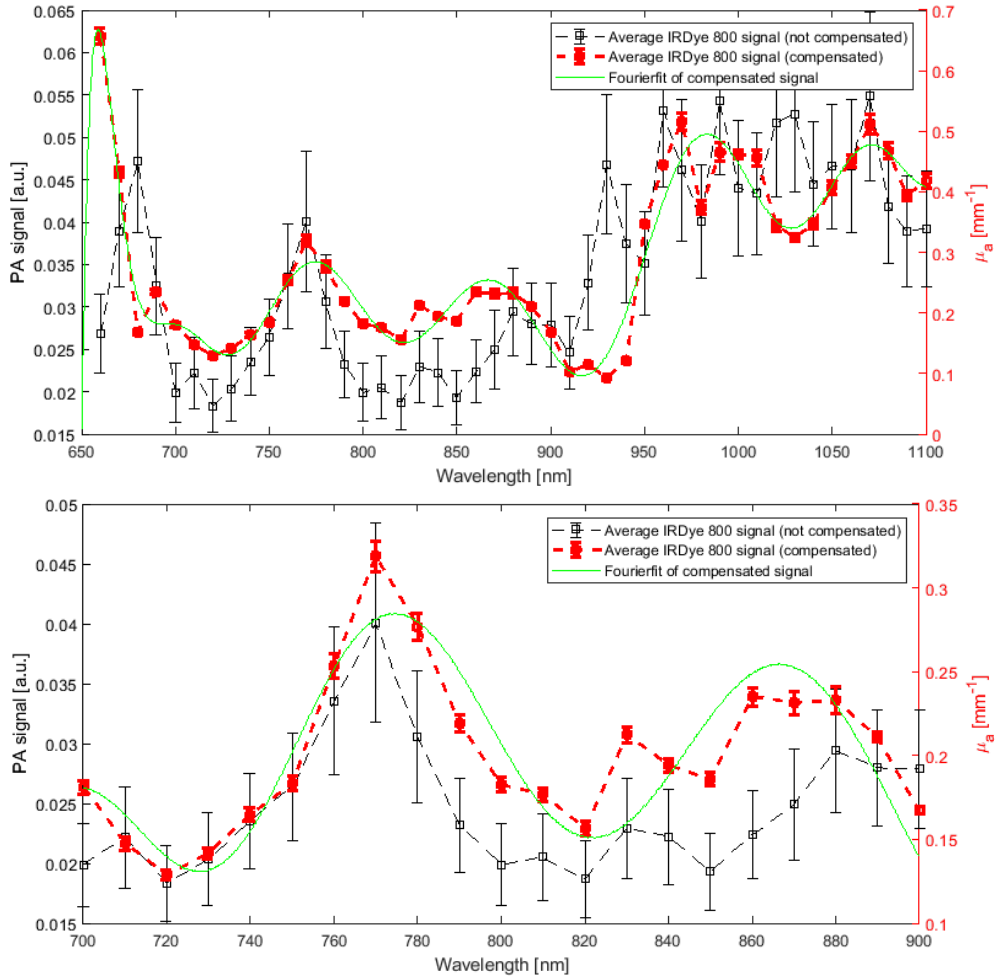

Figure 3.5: *The absorption spectra of IRDye 800 CW (c = 6.82 μM) (full = upper, cropped = lower figure) obtained with photoacoustics at 3 mm depth. The PA signal has been plotted before and after it was compensated for the fluence. A Fourier fit has also been made to show the curve of fluence compensated plot more clearly.*

At first sight, the plots do not resemble the absorption spectra in figure 2.2. However, the absorption peak around 775 nm is visible but there is a large peak at 660 nm that is even higher.

Furthermore, after 900 nm, there is still signal present where there should be no absorption. This can be explained by the laser pulse energy which is lower in that spectral region and thereby increases the values corresponding to the noise resulting in a noisy graph as mentioned in Section 3.1. Since we know that IRDye 800 CW should not show any absorption in that region, the choice has been made to only visualise the spectra from 700 to 900 nm in subsequent plots so that the results become more clear.

3.5 Concentration and imaging depth against the PA signal

To visualise the variation of the compensated PA signal with IRDye 800 concentration and imaging depth, multiple plots are made. See figure 3.6 in which the IRDye 800 concentration with regard to the PA signal is analysed.

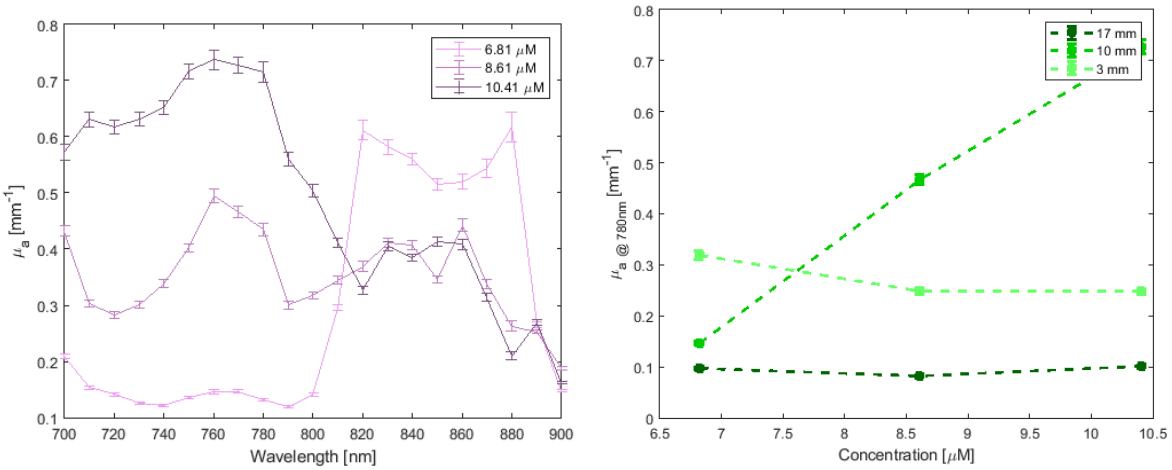

Figure 3.6: *The derived μ_a from the PA signal of IRDye 800 plotted against the wavelength for thee different concentrations at 10 mm imaging depth (left) and μ_a against the concentration plotted for the three imaging depths at λ = 780 nm (right).*

The left graph in figure 3.6 shows the absorption spectra of the three different concentrations of IRDye 800 at 10 mm imaging depth. It is expected that the three plots follow the same outline and that they are evenly spaced apart from each other with the one of 10.41 μM showing the highest and 6.82 μM the lowest signal respectively. This is, however, not entirely the case. The plots do follow the same outline, 10.41 μM is indeed the highest and 6.82 μM is the lowest in most of the spectral region, and the absorption peak around 775 nm is somewhat visible in each plot. After 800 nm, the amplitude of the 8.61 and 10.41 plots is approximately. the same. This is explained by the fact that IRDye 800 does not absorb in that region so the signal only consists of noise Nonetheless, the large deviation in the 8.61 μM plot mentioned in Section 3.3 is also clearly visible in that region.
Furthermore, the right graph shows the concentration plotted against the derived absorption coefficient for the three imaging depths. Here, a linear slope is expected with the same value for each concentration and, again, they are evenly spaced apart in which 3 mm has the highest and 17 mm the lowest signal. This is somewhat true for the values at 6.82 μM However, when the concentration increases, the slope of the 10 mm depth plot is the only positive one. The 8.61 μM values of the 13 and 7 mm plots are even lower than the 6.82 μM values. These results can be explained by the fact that at 3 and 17 mm imaging depth, the measured absorption spectra were almost the same in such a way that there was no clear difference between the μ_a values at different depths. See figure A.1 in appendix A.2. An explanation for this finding is

that at 17 mm, the signal is just too low that it does not exceed above the noise. However, the signal was visible on the live footage on the MSOT device during the measurements. The low signals at 3 mm remain to be discussed. In short, only for an imaging depth of 10 mm, a higher concentration of IRDye 800 seems to increase its PA signal. The fact that the results at the other two imaging depths do not resemble this relation, makes it hard to quantitative conclude anything.

Similar plots can also be made for the imaging depth. See figure 3.7.

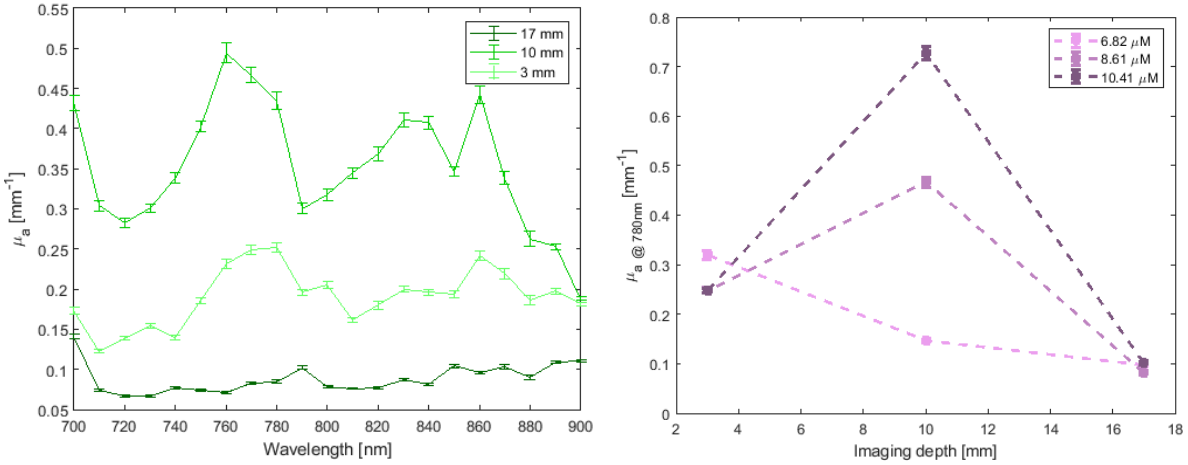

Figure 3.7: *The measured μ_a of IRDye 800 plotted against the wavelength for three imaging depths with 8.61 μM concentration (left) and the μ_a against the imaging depth plotted for the three concentrations at λ = 780 nm (right).*

The left graph in figure 3.7 shows the absorption spectra of IRDye 800 derived from the PA measurements at the three different imaging depths. As mentioned in the previous section, it is expected that the plots follow the same outline and that the 3 mm one has the highest value and the 17 mm the lowest. It was expected that at a deeper imaging depth, the PA signal would decrease since the laser light has a longer optical path length resulting in more scattering and absorption. Furthermore, due to the inverse square law, the amplitude of the acoustic waves is smaller when it reaches the detector. These hypotheses is, again, not entirely the case as the 10 mm plot is clearly the highest of the three which was shown first in figure 3.6. However, unlike the plots in that figure, the signals of the three plots are not approximately the same after 800 nm. This implies that the difference between the plots is really because of the different imaging depths since the noise signals are lower. The low PA signal at 3 mm depth could be explained by the fact that it lies too close to the transducer and therefore too far from its focus not receiving adequate levels of acoustic signals. The right graph, in which $\mu_{a,\lambda=800}$ for the three different concentrations are plotted, shows these results in a different way. Initially, the absorption seems to increase with a deeper imaging depth as the $\mu_{a,\lambda=800}$ value at 10 mm depth is higher than at 3 mm. After that, the signal is decreasing. The exception to this is the plot of 6.82 μM which steadily decreases with a larger imaging depth. These findings were discussed along with the previous figure.

3.6 Calculated concentration vs actual concentration IRDye 800

Finally, the actual concentration of IRDye 800 can be plotted against the calculated concentration derived from the PA measurements. This is done by using the Beer-Lambert law presented

in Eq. 3 since the molar extinction coefficient, ϵ, and μ_a at each wavelength are known. Figure 3.8 shows the correlation at the three different imaging depths for a wavelength of 780 nm in addition to the plot 'y = x' for comparison.

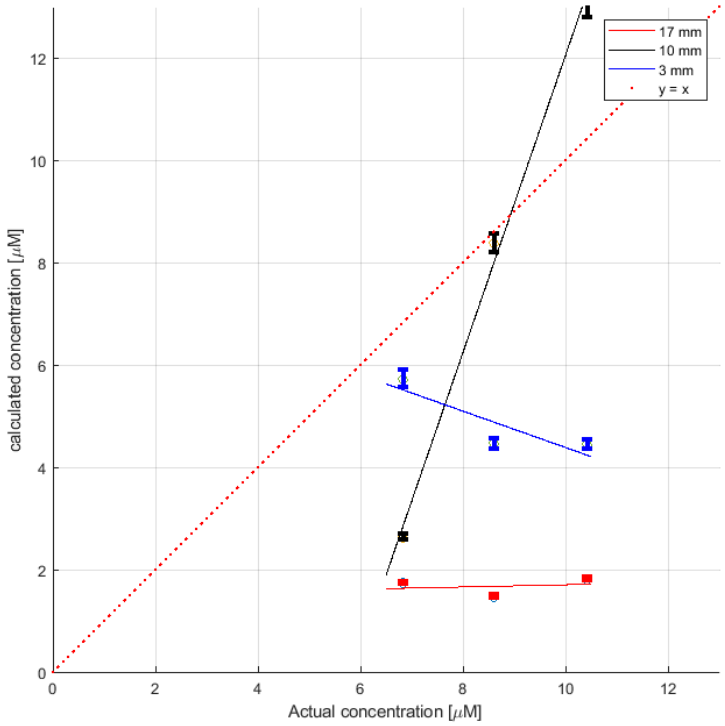

Figure 3.8: *The actual concentration of IRDye 800 plotted with a linear fit against the expected concentration derived from PA measurements at a wavelength of 780 nm.*

When QPAI is fully capable of determining the exact concentration of an IRDye 800 solution, all the plotted points should lie on the equation: y = x. Figure 3.8 shows that this is clearly not the case for any imaging depth. First, almost all the calculated values are lower than the actual ones. Of all the depths, the 10 mm fit seems to most closely resemble the y = x equation since it has a slope of 2.901. However, the plot does not intersect the origin, neither do the others, and the slope of the 3 mm plot is decreasing even. Similar results have been found for other wavelengths, see figure A.2 in appendix A.2. These unusual slopes are probably the result of the same issues discussed in Section 3.5. Due to this, no proportional correlation can be made between the concentration of a chromophore and its PA signal.

4 Discussion

Let it first be stated that multiple external factors have greatly influenced the results of this thesis. Two of the most important of these are the reconstruction method and the pixel selection inside the reconstructed images.

There are multiple methods by which sinograms of photoacoustic measurements can be reconstructed. This paper has used the 'delay and sum' method since it was the easiest to implement and it reconstructs the image the fastest. However, it is generally regarded that the 'time reversal' method gives images of a higher quality in which the contrast is better. [24] Therefore, this method was also looked at. Yet, the corresponding Matlab code was hard to implement in my scripts and the reconstruction time was significantly longer when compared to delay and sum. Furthermore, all the sinograms of the same wavelength at each scan get averaged first (n = approx. 20). This eliminates some of the background noise enhancing the contrast with the signal from inside the tubes to an extent that it was comparable to the quality of the time reversal method. Therefore, the choice has been made to use the Delay and Sum method. However, other reconstruction methods were not looked at and further research must be done to determine their image qualities regarding this experiment.

Similar to reconstruction methods, there are multiple methods to segregate the pixels to be averaged corresponding to the substances inside of the tubes in the reconstructed images. This thesis used an approach in which circles were made with its center corresponding to the pixel with the highest signal of the tube. Then its radius was set to 20 pixels and only the pixel values with an intensity higher than the maximum pixel intensity value were used to calculate the average tube signal This was done to eliminate the background noise from inside of the circle. However, this resulted in a large difference between the used number of pixels between wavelengths and scans, as visible in figure 3.2. This method assumed a uniform distribution of the PA signal of the substance inside of the tube cross-section. This is, however, not entirely the case since a decay of the PA signal throughout the tube is present due to the light absorption. Therefore, another data selection method that took this decay into account is more appropriate for this experiment. This could be done by using a straight line drawn from the bottom part of the transducer to and through the PA signal of a test tube. When this line is drawn correctly for each tube, the relative decay caused by the absorption inside the tube should be the same for each condition since the optical path inside the tubes is the same.

As mentioned in Section 3.2, the laser energy differs for each wavelength and even for each sweep number. The data were compensated for this difference by dividing each sinogram by its corresponding laser energy value. After that, the images were reconstructed and the data extracted from the ROIs. Yet, when the fluence compensation scalars are made from the reference tube signals, they are already compensated for the laser energy. So when these scalars are multiplied with the values corresponding to the test tube, which are also compensated for the laser energy, they get compensated twice. So most of the calculated μ_a values of the IRDye 800 are too low. This could explain the lower calculated values of the concentration in figure 3.8 in comparison with the actual concentrations. To solve this issue, the compensation method should be reworked in such a way that this double compensation does not occur. This can be done by segregating the pixel values corresponding to the test tube before the PA signal gets compensated by the laser energy.

One of the major deviations from the initial measurement protocol was the unavailability of intralipid that serves as a scattering medium mimicking soft tissue. This unavailability was not known of until shortly before the day that the measurements were taken at the UMCG. Therefore, improvisation was needed to solve this issue. Because milk contains significant amounts of fat, like intralipid, and it is widely available, the choice to use that was quickly made. The major downside of this approach was that the scattering properties of milk were unknown and had to be determined afterwards. Another alternative that could have been used was titanium oxide since those optical properties were known but it was also not available for the moment. Nonetheless, the optical properties of the whole milk that was used had to be characterised afterwards which was done with the inverse adding doubling method. However, due to the use of an incompatible material, polystyrene, as the reference sample for this method, the scattering properties could not be retrieved. This characterisation could, of course, be conducted again with a different reference sample but due to time constraints, that was not feasible. Even a quick literature search did not suffice in giving adequate approximations for the reduced scattering coefficient. Therefore, it must be noted that all the results presented in this thesis do not represent a situation in which the scattering of light in soft tissue is mimicked. In all, this part of the thesis took more time than initially planned which resulted in there being less time available for other aspects of the data analysis. For further experiments, I recommend using intralipid since it is a more standard approach and if other substances are used for a particular reason, make sure the optical properties are known at each measured concentration.

Chapter 3 showed that the PA signal-derived absorption spectra of IRDye 800 does not entirely resemble the spectra from the spectrophotometer measurements. The characteristic absorption peak at 775 nm is somewhat visible but the absorption should remain dormant after approx. 850 nm. This is obviously not the case for either the uncompensated or the compensated PA spectra. The general outline of the uncompensated and the compensated plots are highly similar and mostly only differ by scale. Therefore, improving the preparations for image reconstruction (i.e. sweep average, laser energy compensation, etc.) and data selection in the ROIs will likely contribute the most to making the PA signal-derived spectra resemble the actual one closer. Furthermore, it is assumed that the signal in the spectral region above 850 nm, which is only background noise, is the result of the corresponding low laser energy values and that the compensation actually increases the noise. However, the energy values are approx. 0.9 mJ after 950 nm which should not increase the noise by a significant amount. Therefore, it remains disputed what exactly causes the PA signal in the region.

Improving the method of retrieving the absorption spectra could also enhance the poorly defined relationship between the IRDye 800 concentration and imaging depth with the PA signal and the actual versus the expected concentration in addition to the double laser energy compensation discussed previously. Figure 3.8 clearly shows that the relation derived from the 3 and 17 mm imaging depth does not hold and that only at 10 mm, a linear relation could be seen. Other results also showed deviations of 3 and 17 mm imaging depth plots. Therefore, this thesis questions the validity of the results at these depths Remarkably, all the calculated concentrations were in the same order of magnitude as the actual ones, only a few units lower. Therefore, it is assumed that the method of calculating the concentrations from the PA signal values is not inherently wrong.

It must be noted that a large portion of the available time to work on this thesis was used to prepare the experiment as many parameters and other aspects had to be researched and

determined. Furthermore, practice experiments were conducted beforehand with the self-build experiment configuration at the Department of Biomedical Photonic Imaging at the University of Twente to get acquainted with PA measurements and to characterise the tubes. Furthermore, many hours have been spent in the chemical lab making the different dilutions of India Ink, IRDye 800, and whole milk to measure them with the spectrophotometer. These preparations took more time than initially planned so there was less time available for the data analysis. This resulted in the fact that the first approach on how to analyse the results with came to mind, was used most of the time, and less time was spent on constructing and applying different ones. One example of this was the method of fluence correction. This thesis used the same approach as Cas [16] instead of developing its own. If more time was available, other methods could be investigated to if they gave different results.

The initial goal of this thesis was to determine if it is possible to derive the concentration of lipids inside of a *ex vivo* carotid artery plaque. One plaque sample was available to take measurements with. However, due to time constraints at the UMCG, it was not possible to conduct such measurements. Furthermore, only a metal needle was available to hold the plaque stationary inside of the tank which would have given a large artefact in the reconstructed image. When measurements with a plaque are taken, no highly absorbing or reflecting materials should be in close proximity to reduce imaging artefacts. Furthermore, a different substance other than India Ink which may more closely resemble substances found in artery blood could be used as a reference to correct the fluence with.

5 Outlook

The aim of this thesis was to investigate if it is possible to determine the concentration of a chromophore with unknown properties via photoacoustic imaging by correcting for the optical fluence implement and this in carotid plaque imaging to determine the plaque stability. The NIR absorber IRDye 800 CW was used along with India Ink as a reference to compensate for the fluence. This thesis showed that QPAI is capable of determining this information to a certain extent. However, the relationships between the investigated parameters have not been found quantitatively but, the calculated concentrations of IRDye 800 were in the same order of magnitude. Further research on compensating with the laser energy and data extraction from the tubes would most likely lead to newer insights and, hopefully, more adequate quantitative results. Therefore, I predict QPAI has the potential in developing novel techniques in which *in vivo* carotid artery plaques, and even other biological tissues, can be characterised.

Acknowledgements

I would first like to thank Francis Kalloor Joseph PhD for providing me this assignment. His guidance and supervision were very helpfull and he brought new insights to problems I encountered. Anjali Thomas PhD helped with every experiment and the coding. She also provided feedback on my work which I am very grateful for. Dr. Bruno de Santi also needs to be highlighted as he was willing to be part of my graduation committee.

Special thanks also need to be given to Jasper Vonk from the UMCG. Without him, the experiment would not be be possible in the way it is.now. He made it possible to use the MSOT device for two days and provided the corresponding guidance.

Then, I would like to thank all the members of the Biomedical Photonic Imaging group of the University of Twente. They welcomed me with open arms and I have enjoyed my time here. I would like to thank specifically Tom Knop BSc for helping with the optical lab instrumentation, Wilma Peterson for helping with the chemical lab instrumentation (specifically the spectrophotometer), dr.ir. David Thompson and Rianne Bulthuis BSc for their help with the milk characterisation and Eline Zoetelief for providing feedback during the short update meeting.

Last but not least, I would like to thank all the students with whom I shared the office with the last ten weeks. They ensured a positive ambience and were open to provide support when needed.

References

[1] Carotid Stenosis; 2023. [Online; accessed 18. Jun. 2023]. Available from: https://www.templehealth.org/services/conditions/carotid-stenosis.

[2] The top 10 causes of death. World Health Organization: WHO; 2020. Available from: https://www.who.int/news-room/fact-sheets/detail/the-top-10-causes-of-death.

[3] Sanz J, Fayad ZA. Imaging of atherosclerotic cardiovascular disease. Nature. 2008 Feb;451:953–957. doi:10.1038/nature06803.

[4] Nighoghossian N, Derex L, Douek P. The Vulnerable Carotid Artery Plaque. Stroke. 2005 Dec. doi:10.1161/01.0000190895.51934.43.

[5] Steinkamp PJ, Vonk J, Huisman LA, Meersma GJ, Diercks GFH, Hillebrands JL, et al. VEGF-Targeted Multispectral Optoacoustic Tomography and Fluorescence Molecular Imaging in Human Carotid Atherosclerotic Plaques. Diagnostics. 2021 Jul;11(7):1227. doi:10.3390/diagnostics11071227.

[6] Huisman LA, Steinkamp PJ, Hillebrands JL, Zeebregts CJ, Linssen MD, Jorritsma-Smit A, et al. Feasibility of ex vivo fluorescence imaging of angiogenesis in (non-) culprit human carotid atherosclerotic plaques using bevacizumab-800CW. Sci Rep. 2021 Feb;11(1):2899. doi:10.1038/s41598-021-82568-8.

[7] Kruizinga P, van der Steen AFW, de Jong N, Springeling G, Robertus JL, van der Lugt A, et al. Photoacoustic imaging of carotid artery atherosclerosis. J Biomed Opt. 2014 Nov;19(11):110504. doi:10.1117/1.JBO.19.11.110504.

[8] Beard P. Biomedical photoacoustic imaging. Interface Focus. 2011 Aug;1(4):602–631. doi:10.1098/rsfs.2011.0028.

[9] Cox B, Laufer JG, Arridge SR, Beard PC. Quantitative spectroscopic photoacoustic imaging: a review. J Biomed Opt. 2012 Jun;17(6):061202. doi:10.1117/1.JBO.17.6.061202.

[10] Allen TJ, Hall A, Dhillon AP, Owen JS, Beard PC. Spectroscopic photoacoustic imaging of lipid-rich plaques in the human aorta in the 740 to 1400 nm wavelength range. J Biomed Opt. 2012 Jun;17(6):061209. doi:10.1117/1.JBO.17.6.061209.

[11] Wang B, Su JL, Amirian J, Litovsky SH, Smalling R, Emelianov S. Detection of lipid in atherosclerotic vessels using ultrasound-guided spectroscopic intravascular photoacoustic imaging. Opt Express. 2010 Mar;18(5):4889. doi:10.1364/OE.18.004889.

[12] Tarvainen T, Vauhkonen M, Kolehmainen V, Kaipio JP. Finite element model for the coupled radiative transfer equation and diffusion approximation. Int J Numer Methods Eng. 2006 Jan;65(3):383–405. doi:10.1002/nme.1451.

[13] Banerjee S, Sharma SK. Use of Monte Carlo simulations for propagation of light in biomedical tissues. Appl Opt. 2010 Aug;49(22):4152–4159. doi:10.1364/AO.49.004152.

[14] Bal G, Ren K. Multi-source quantitative photoacoustic tomography in a diffusive regime. Inverse Prob. 2011 Jun;27(7):075003. doi:10.1088/0266-5611/27/7/075003.

[15] Sivaramakrishnan M, Maslov K, Zhang HF, Stoica G, Wang LV. Limitations of quantitative photoacoustic measurements of blood oxygenation in small vessels. Phys Med Biol. 2007 Feb;52(5):1349. doi:10.1088/0031-9155/52/5/010.

[16] Weernink CJH. Light fluence marker for quantitative photoacoustic imaging; 2022. Available from: `http://essay.utwente.nl/91981/`.

[17] Bosschaart N, Edelman GJ, Aalders MCG, van Leeuwen TG, Faber DJ. A literature review and novel theoretical approach on the optical properties of whole blood. Lasers Med Sci. 2014 Mar;29(2):453–479. doi:10.1007/s10103-013-1446-7.

[18] Yaroslavsky AN, Yaroslavsky IV, Goldbach T, Hans-Joachim Schwarzmaier MD. Optical properties of blood in the near-infrared spectral range. In: Proceedings Volume 2678, Optical Diagnostics of Living Cells and Biofluids. vol. 2678. SPIE; 1996. p. 314–324. doi:10.1117/12.239516.

[19] Jacques SL. Optical properties of biological tissues: a review. Phys Med Biol. 2013 Jun;58(11):37–61. doi:10.1088/0031-9155/58/11/R37.

[20] Rajian JR, Carson PL, Wang X. Quantitative photoacoustic measurement of tissue optical absorption spectrum aided by an optical contrast agent. Opt Express. 2009 Mar;17(6):4879. doi:10.1364/oe.17.004879.

[21] Zhao Z, Myllylä R. Scattering photoacoustic study of weakly-absorbing substances in aqueous suspensions. Journal de Physique IV (Proceedings). 2006 Jan;137:385–390. doi:10.1051/jp4:2006137072.

[22] Prahl S. Optical Property Measurements Using the Inverse Adding Doubling Program. ResearchGate. 2011 Oct. Available from: `https://www.researchgate.net/publication/254428856_Optical_Property_Measurements_Using_the_Inverse_Adding_Doubling_Program`.

[23] Aernouts B, Van Beers R, Watté R, Huybrechts T, Lammertyn J, Saeys W. Visible and near-infrared bulk optical properties of raw milk. J Dairy Sci. 2015 Oct;98(10):6727–6738. doi:10.3168/jds.2015-9630.

[24] Subochev PV, Volkov GP, Perekatova VV, Turchin IV. Comparing reconstruction algorithms for the 2D optoacoustic tomography of biological tissues. Bull Russ Acad Sci: Phys. 2016 Oct;80(10):1237–1241. doi:10.3103/S106287381610018X.

A Appendices

A.1 Experiment protocols

Measurement protocol

1. Make sure the door of the room is tightly closed so the interlock can be turned on.
2. Turn on the iThera Mecial MSOT acuity device.
3. Set the device to 'clinical mode'.
4. Select the program: '2D concave 660-1130 nm'.
5. Fill the tank with 9 liters of water and place it under the the probe.
6. Add a certain India Ink and intralipid/whole milk so that it mimics the optical properties of soft tissue.
7. Fill the reference tube with the India Ink dilution
8. Fill the test tube with the desired IRDye 800 dilution
9. Insert both tubes into the holder at the desired measuring depth by pushing them through the holes.
    - The next to closest holes to the transducer is 3 mm, the holes below that 10 and below that 17.
    - Make sure that the (horizontal) distance between the tubes is two holes (14 mm).
10. Secure the tube holder to the probe and lower it into the water.
11. Close the lid of the cabinet where the probe and tank are located (note: if the lid is not closed, every person in the room must wear appropriate laser safety glasses if a measurement is being conducted).
12. Initiate the laser by pressing down on the food pedal.
13. Press 'View' on the device.
14. Two live footages can now be seen: the US signal (left) and PA signal (right).
15. Check if both tubes are visible on the US signal and if they are at the exact same depth. If not, try to adjust it manually by stretching one (note: put on the laser safety glasses when working with the lid open).
16. Start a scan by pressing 'Record' and measure for about 30 seconds.
17. Repeat this two times to get triplo results.
18. Repeat steps 9 through 17 for every depth.
19. Repeat steps 8 through 18 for every IRDye 800 dilution (note. thoroughly clean the test tube first when swithing to another concentration).
20. 27 scans in total should have been made by now.

Milk characterisation protocol

Note: this protocol is written in such a way that it assumes that the measurements of the the previous protocol have been conducted just before starting the milk characterisation.

1. Choose an IRdye 800 concentration and imaging depth you would like to take the measurements at.
2. Note the concentration of milk in the water tank
3. Make two measurements (recordings) of ca. 20-30 seconds.
4. Add 10 mL of milk to the tank
5. Repeat steps 2 through 4 fifteen times.
6. 32 scans in total should have been made by now.

A.2 More data analysis figures

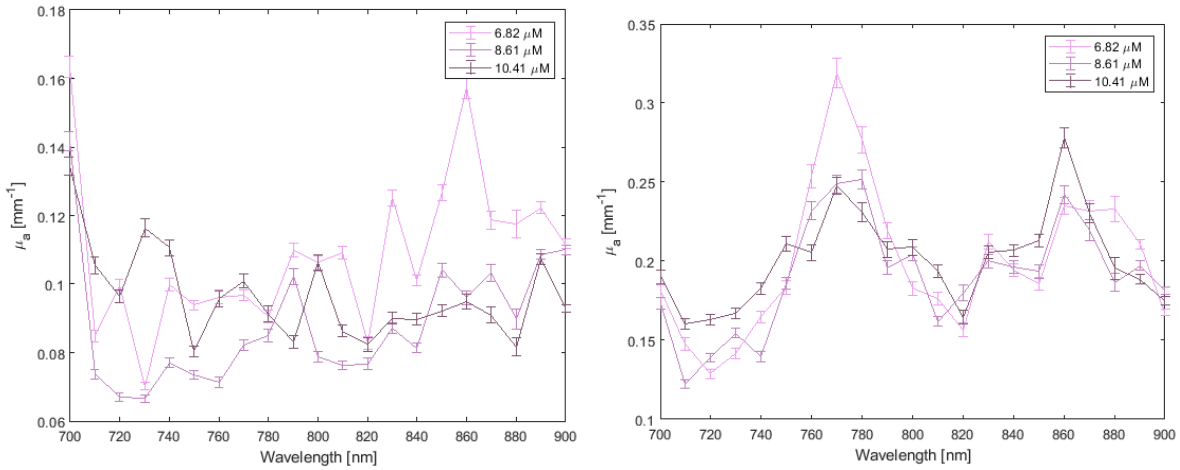

Figure A.1: *The derived μ_a from the PA signal of IRDye 800 plotted against the wavelength for three different concentrations at 17 (left) and 3 mm imaging depth (right).*

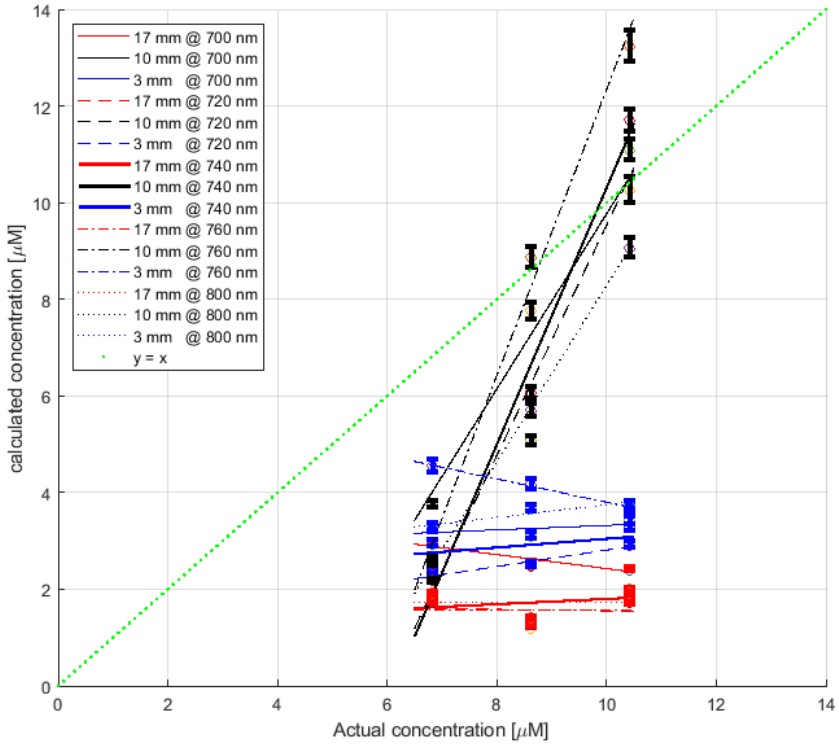

Figure A.2: *The actual concentration of IRDye 800 plotted with a linear fit against the expected concentration derived from PA measurements at multiple wavelengths.*

A.3 MSOT_to_MAT_converter.py

```
import os
from ilib.datamodel import iScan, iSignal
import numpy as np
import scipy.io


## Start of the code


# Define the folder path where the .msot files are located
folder_path = "C:/Users/Youri Meevis/Desktop/MSOT Python convertor/Raw milk charactisation .msot  files (UMCG day 2)"

# Define the file extension to search for
file_extension = ".msot"

# Iterate over the root folder and its subfolders
for root, dirs, files in os.walk(folder_path):
    for file in files:
        if file.endswith(file_extension):
            file_path = os.path.join(root, file)

            # Collecting the RF-data (a.k.a. the sinograms)
            scan = iScan(file_path)
            signal = iSignal.from_scan(scan)
            sinograms = signal.view(np.ndarray) # 4D-structure of the sinograms of every sweep of each wavelength

            # Saving other useful parameters
            senspos = scan.Probe.get_sensors() # sensor position [mm mm]
            laserenergy = signal.LaserEnergy   # list of laser energy values of each wavelength of each sweep [mJ]
            wavelengths = signal.Wavelength    # wavelengths [nm]
            sweepnumbers = signal.SweepIndex   # amount of sweeps per wavelength

            # Generate the new file name and path
            new_file_name = os.path.splitext(file)[0] + ".mat"
            new_file_path = os.path.join(os.path.dirname(os.path.dirname(root)), new_file_name)

            # Saving the sinograms and other parameters in a .mat file
            scipy.io.savemat(new_file_path, {'sinogram': sinograms, 'sensor_pos': senspos, 'laser_energy':
                                             laserenergy, 'wavelength': wavelengths, 'sweeps': sweepnumbers})

            print(f"Processed file: {new_file_path}")
```

```
print("All files processed successfully.")
```

A.4 PA_DASreconstruction_and_ROIs_collection.m

```
%% ============================================== %%
%   PA_DASreconstruction_and_ROIs_collection.m    %
%% ============================================== %%

% This script uses the delay and sum method to reconstruct photoacoustic images and
% automaticlly calculates the average PA-value of two circular ROIs
% Made by: Anjali thomas PhD & Youri Meevis

% Input:  .mat files of a converted .msot file retreived from 'MSOT_to_MAT_convertor.py' (three files for the same condition)
% Output: table with the average PA-signal values of the two ROIs at each wavelength and other usefull results saved as a .
      mat file for each scan

clear all;
close all;
clc;

%% ---------------- Start of the code--------------------

%% Select the conditon by changing 'depth' and 'concentration'
 depth = 3;              % 1 = 17 mm       2 = 10 mm      3 = 3 mm
 concentration = 3;      % 1 = 6.82  M      2 = 8.62  M     3 = 10.41  M

if depth == 1
    if concentration == 1
        n = 1;
    elseif concentration == 2
        n = 16;
    elseif concentration == 3
        n = 19;
    end
elseif depth == 2
    if concentration == 1
        n = 4;
    elseif concentration == 2
        n = 13;
    elseif concentration == 3
        n = 22;
    end
elseif depth == 3
    if concentration == 1
        n = 7;
    elseif concentration == 2
        n = 10;
    elseif concentration == 3
        n = 25;
    end
end

n2 = n+1;
n3 = n+2;

scan1 = "Scan_" + (n) + ".mat";    % Files retrieved from MSOTdataconvertor.py
scan2 = "Scan_" + (n+1) + ".mat";
scan3 = "Scan_" + (n+2) + ".mat";


for s = 1:3                        % Each condition has 3 scans
scan =  "Scan_" + n + ".mat";

load (scan)



%% Prelocating space for results that needs to be saved in the end
n_wavelength = 1;
all_laser_energies = zeros(48,1);         % There are always 48 wavelengths
all_laser_energies_std = zeros(48,1);
no_used_pixels_in_ROI_ref = zeros(48,1);
no_used_pixels_in_ROI_test = zeros(48,1);

for wavelength = 660:10:1130
wavelength_index = (wavelength-650)/10;
no_sweeps = sweeps(end) - 1;
laser_energy_indeces = wavelength_index + 48*(0:no_sweeps-1); % Indeces for all the laser energies corresponding to 1
      wavelength in one scan
laser_energies = laser_energy(laser_energy_indeces);          % All the laser energies values correspdonding to 1 wavelength
      in one scan
laser_energy_mean = mean(laser_energies);                     % The average laser energy value of 1 wavelength in one scan
laser_energy_std = std(laser_energies);



%% Indexing the correct sinogram(s)
allsinograms = sinogram(:,wavelength_index,:,:);      % Extracting all the sinograms of 1 wavelength
allsinograms_3D = squeeze(allsinograms);              % Making it a 3D-array
```

```
83
84  sinograms_corrected = zeros(no_sweeps, 256, 2030);                                  % Prelocating space for the all the
        sinograms taking the sweep number into account
85  for sweep = 1:no_sweeps                                                             % Determing the sweep number
86     laser_energy_1D = laser_energies(sweep);                                         % Corresponding laser energy value of
           the sinogram
87     sinogram_2D = squeeze(allsinograms_3D(sweep,:,:));                               % 2D sinogram
88     sinogram_2D = double(sinogram_2D)./laser_energy_1D;                              % Compensating the sinogram for the
           laser energy
89     sinograms_corrected(sweep,:,:) = double(sinogram_2D) - mean(sinogram_2D, 'all'); % Normalzing the sinogram
90  end
91  sinogram_final = squeeze(mean(sinograms_corrected));                                % Average sinogram of all the sweeps
        before filtering
92
93
94
95  %% 1D filtering of the sinogram
96  load FilterCoff.mat                  % Loading the filter parameters
97  a = 1;                               % Filter value
98
99  SinogramFilt = zeros(256,2030);      % Preolcating space
100 for i = 1:size(sinogram_final)
101  SinogramFilt(i,:) = filter(b,a,double(sinogram_final(i,:))); % Filtering the sinogram each column at the time
102 end
103
104 SinogramFilt(:,1:size(sinogram_final)) = 0;                    % Set initial values to zero
105 [no_ScanElements, no_samp] = size(SinogramFilt);               % Acquiring parameters for the image reconstruction
106
107
108
109 %% Load tranducer coordinates (x- and z-coordinates)
110  Coordinate_data = sensor_pos;              % Loading the transducer coordinates
111      ze = -1*Coordinate_data(:,3).*10^3;    % Millimeter to meter converstion
112      xe = Coordinate_data(:,1).*10^3;
113      ze = ze+40;                            % Adjusting the position of sensor (z=0)
114      Chord = xe(1,1) - xe(256,1);           % Length of chord
115
116
117
118 %% Defining Medium and transducer ptoprtyird
119 soundspeed = 1480;                                      % medium sound speed [m/s]
120 cutoff_angle_degree = 30;                               % cutoff angle [degrees]
121 cutoff_angle_radian = cutoff_angle_degree*2*pi/360;     % cutoff angle [radians]
122
123 samp_freq_Hz = 40e6;                    % sampling frequency
124 RadiusOfCurvature = 40;                 % probe radius of curvature
125 soundspeed_mm = soundspeed*10^3;        % medium sound speed [mm/s]
126 zStep = soundspeed_mm/samp_freq_Hz;     % axial step size [mm]
127
128
129
130 %% Defining Reconstruction area
131 x_grid_lines = 1000;     % The image will be a 1000x1000 pixel grid
132 z_grid_lines = 1000;
133
134 depth_mm = no_samp * soundspeed_mm / samp_freq_Hz;         % Length of reconstruction in z-direction
135 breadth_mm = Chord+2;                                      % Length of the chord+2mm
136
137
138
139 %% Defining Grid and Coordinates system
140 x_step = breadth_mm/(x_grid_lines-1);
141 z_step = depth_mm/(z_grid_lines-1);
142 x_grid = -breadth_mm/2:x_step:breadth_mm/2;
143 z_grid = 0:z_step:depth_mm;
144
145 [x_coord,z_coord] = meshgrid(x_grid,z_grid);
146
147
148
149 %% Using DAS to reconstruct an image from the sinogram
150 tic                                         % Start timer
151
152 image_recon = zeros(z_grid_lines, x_grid_lines);  % Precolacting array space for the reconstructed image
153
154 for i = 1:z_grid_lines
155     for j = 1:x_grid_lines
156         sum = 0;
157
158         for k = 1:no_ScanElements
159             dist = sqrt((x_coord(i,j)-xe(k))^2+(z_coord(i,j)-ze(k))^2);
160             time = max(1,round(dist*samp_freq_Hz/soundspeed_mm));
161
162             angle = abs(atan((x_coord(i,j)-xe(k))/(z_coord(i,j)-ze(k))));
163
164             if time <= no_samp && angle <= cutoff_angle_radian
165                 sum = sum + SinogramFilt(k,time) ;
166             end
167
168         end
169         image_recon(i,j) = sum;
170     end
171 end
```

```
172
173 image_recon = (image_recon/no_ScanElements); % Reconstructed image
174 image_recon = abs(hilbert(image_recon));     % Hilbert transforming the image
175
176 toc                                          % Stop timer
177
178
179
180 %% Selecting the ROIs
181 radius = 20;       % Radius of both ROIs
182
183 x_cut_1 = 200;     % Horizontal cut of the reconstructed image to show the tubes better
184 x_cut_2 = 800;
185
186
187 % The exact postion of each tube is not the same for each condition but this gets corrected automatically
188  if depth == 1
189      d_cut_1 = 600;                     % Vertical cut of the reconstructed image to show the tubes better
190      d_cut_2 = 800;
191      if concentration == 1
192          center_refPixels = [191 102];  % Center coordinates of the reference tube
193          center_testPixels = [395 92];  % Center coordinates of the test tube
194      elseif concentration == 2
195          center_refPixels = [182 91];
196          center_testPixels = [379 90];
197      elseif concentration == 3
198          center_refPixels = [189 96];
199          center_testPixels = [370 96];
200      end
201
202  elseif depth == 2
203      d_cut_1 = 500;
204      d_cut_2 = 700;
205      if concentration == 1
206          center_refPixels = [194 76];
207          center_testPixels = [359 74];
208      elseif concentration == 2
209          center_refPixels = [178 92];
210          center_testPixels = [385 93];
211      elseif concentration == 3
212          center_refPixels = [190 87];
213          center_testPixels = [400 83];
214      end
215
216  elseif depth == 3
217      d_cut_1 = 400;
218      d_cut_2 = 600;
219      if concentration == 1
220          center_refPixels = [187 105];
221          center_testPixels = [358 100];
222      elseif concentration == 2
223          center_refPixels = [189 105];
224          center_testPixels = [380 100];
225      elseif concentration == 3
226          center_refPixels = [189 116];
227          center_testPixels = [375 117];
228      end
229  end
230
231 % Displaying the reconstructed image
232 figure()
233 fig.WindowState = 'maximized';
234 imagesc(image_recon(d_cut_1:d_cut_2,x_cut_1:x_cut_2))
235 impixelinfo
236 colormap(hot);
237 colorbar;
238 title(['Reconstructed PA image \lambda = ' num2str(wavelength) 'nm']);
239 axis('equal');
240 axis tight;
241 xlabel('Lateral cross section [mm]')
242 ylabel('Imaging depth [mm]')
243 hold on
244
245 %% Calculating the PA signals of both tubes
246 % Reconfigurating the grid
247 image_recon = image_recon(x_cut_1:x_cut_2,d_cut_1:d_cut_2);
248 new_x_grid_lines = x_cut_2 - x_cut_1;
249 new_z_grid_lines = d_cut_2 - d_cut_1;
250 [x, z] = meshgrid(1:new_x_grid_lines, 1:new_z_grid_lines);
251
252 % Drawing the ROIs onto the reconstructed image
253 theta = linspace(0, 2*pi, 100);
254 circle_ref_X = center_refPixels(1) + radius * cos(theta);
255 circle_ref_Z = center_refPixels(2) + radius * sin(theta);
256 plot(circle_ref_X, circle_ref_Z, 'b', 'LineWidth', 2);
257 hold on;
258 theta = linspace(0, 2*pi, 100);
259 circle_test_X = center_testPixels(1) + radius * cos(theta);
260 circle_test_Z = center_testPixels(2) + radius * sin(theta);
261 plot(circle_test_X, circle_test_Z, 'b', 'LineWidth', 2);
262
263 % Calculating the distances of the center of the ROIs to the origin
264 distances_ref = sqrt((x - center_refPixels(1)).^2 + (z - center_refPixels(2)).^2);
```

```
distances_test = sqrt((x - center_testPixels(1)).^2 + (z - center_testPixels(2)).^2);

% Indexing the pixels inside of the tube
pixels_in_ROI_ref = distances_ref <= radius;
pixels_in_ROI_test = distances_test <= radius;

% Determining all the pixels inside of the ROIs
dataROI_ref = image_recon(pixels_in_ROI_ref);
dataROI_test = image_recon(pixels_in_ROI_test);

dataROI_ref = dataROI_ref(:);
dataROI_test = dataROI_test(:);


% Removing the pixel values with a lower value than half of the maximum
% value
max_ref = max(dataROI_ref);
ref_threshold = max_ref*0.5;
dataROI_ref_filtered = dataROI_ref(dataROI_ref >= ref_threshold);

max_test = max(dataROI_test);
test_threshold = max_test*0.5;
dataROI_test_filtered = dataROI_test(dataROI_test >= test_threshold);


% Calculating the average PA signal of the ROIs.
ref_avgPAS = mean(dataROI_ref_filtered);   % Average reference value
test_avgPAS = mean(dataROI_test_filtered); % Average test value

ref_stdPAS = std(dataROI_ref_filtered);    % Standarddeviation value for reference tube
test_stdPAS = std(dataROI_test_filtered);  % Standarddeviation value for test tube


% Collecting the wavelength energies
all_laser_energies(n_wavelength) = laser_energy_mean;
all_laser_energies_std(n_wavelength) = laser_energy_std;
no_used_pixels_in_ROI_ref(n_wavelength) = length(dataROI_ref_filtered);
no_used_pixels_in_ROI_test(n_wavelength) = length(dataROI_test_filtered);


%% Storing the results in the 'results' table
results.Wavelength(n_wavelength) = wavelength;
results.Average_reference_tube_signal(n_wavelength) = ref_avgPAS;
results.Average_test_tube_signal(n_wavelength) = test_avgPAS;
results.std_reference_tube_signal(n_wavelength) = ref_stdPAS;
results.std_test_tube_signal(n_wavelength) = test_stdPAS;
results.laser_energies(n_wavelength) = laser_energy_mean;
results.laser_energies_std(n_wavelength) = laser_energy_std;
results.no_used_pixels_in_ROI_ref = no_used_pixels_in_ROI_ref;
results.no_used_pixels_in_ROI_test = no_used_pixels_in_ROI_test;

disp(results);



n_wavelength = n_wavelength+1;
end

% Saving the results inside a .mat corresponding to its scan
finalfileName = erase(scan, ".mat") + '_ROIs_average_results.mat';
save(finalfileName, 'results');

disp('File finished')

n = n+1;
end
```

A.5 PA_ROIs_analysis.m

```
%% ==================================== %%
%         PA_ROIs_analysis.m            %
%% ==================================== %%

% This script compensates the test tube PA-signal value with the reference
% tube PA-signal value to retrieve the absorption spectrum of IRDye 800 CW

% Inputs:  - 3 .mat files retrieved from the 'PA_DASreconstruction_and_ROIs_collection.m' script with the same experimental conditions
%             'depth' and 'concentration' value corresponding to the conditions
%          - 2 .txt files of the 0.59 mu_a @ 800 nm India Ink dilution absorbtion measurements with a spectrophotometer + baseline
% Output: .mat file containing the fluence compensated array of the test tube signal [mu_a]


clc
clear all
```

```
close all


%% ---------------- Start of the code-------------------- %%

% Select the wavelenght range for the plots (min = 660, max = 1130)
wavelength_start = 660;   % Lowest wavelength on the plots
wavelength_stop = 1130;   % Highest wavelength on the plots

start = (wavelength_start-650)/10; % Corresponding index
stop = (wavelength_stop-650)/10;


%% Select the conditon by changing 'depth' and 'concentration'
depth = 3;              % 1 = 17 mm       2 = 10 mm      3 = 3 mm
concentration = 1;      % 1 = 6.82  M      2 = 8.61  M     3 = 10.41  M
if depth == 1
    if concentration == 1
        n = 1;
    elseif concentration == 2
        n = 16;
    elseif concentration == 3
        n = 19;
    end
elseif depth == 2
    if concentration == 1
        n = 4;
    elseif concentration == 2
        n = 13;
    elseif concentration == 3
        n = 22;
    end
elseif depth == 3
    if concentration == 1
        n = 7;
    elseif concentration == 2
        n = 10;
    elseif concentration == 3
        n = 25;
    end
end

n2 = n+1;
n3 = n+2;

scan1 = "Scan_" + n + "_ROIs_average_results.mat";   % Files retrieved from PA_DASreconstruction_and_ROIs_collection.m
scan2 = "Scan_" + n2 + "_ROIs_average_results.mat";
scan3 = "Scan_" + n3 + "_ROIs_average_results.mat";



%% Average PA signal of the tubes (3 measurements)
load (scan1)
wavelengths = results.Wavelength;
m1_ref = results.Average_reference_tube_signal;  % Reference tube
m1_test = results.Average_test_tube_signal;      % Test tube
m1_ref_std = results.std_reference_tube_signal;
m1_test_std = results.std_test_tube_signal;

load (scan2)
m2_ref = results.Average_reference_tube_signal;
m2_test = results.Average_test_tube_signal;
m2_ref_std = results.std_reference_tube_signal;
m2_test_std = results.std_test_tube_signal;

load (scan3)
m3_ref = results.Average_reference_tube_signal;
m3_test = results.Average_test_tube_signal;
m3_ref_std = results.std_reference_tube_signal;
m3_test_std = results.std_test_tube_signal;
m3_used_pixels_ref = results.no_used_pixels_in_ROI_ref;
m3_used_pixels_test = results.no_used_pixels_in_ROI_test;

% Plotting the IRDye 800 signal the 3 scans
figure(1)
errorbar(wavelengths,m1_test,m1_test_std)
hold on
errorbar(wavelengths,m2_test,m2_test_std)
hold on
errorbar(wavelengths,m3_test,m3_test_std)
legend('Measure. 1','Measure. 2','Measure. 3')
title('IRDye 800 (test) tube PA signal values of the three measurements')
xlabel('Wavelength [nm]')
ylabel('Absorption [a.u.]')

% calculating the average for the condition
ref_avg = (m1_ref+m2_ref+m3_ref)/3;                          % Average reference tube (India Ink) signal value over 3 scans
test_avg = (m1_test+m2_test+m3_test)/3;                      % Average test tube (IRDye 800) signal value over 3 scans
ref_avg_std = (m1_ref_std + m2_ref_std + m3_ref_std)/3;      % Average reference tube (India Ink) signal standardeviation
      over 3 scans
test_avg_std = (m1_test_std + m2_test_std + m3_test_std)/3;  % Average test tube (IRDye 800) signal standardeviation over 3
      scans

```

```
% Plotting the average IRdye 800 signal
figure()
errorbar(wavelengths,ref_avg,ref_avg_std)
hold on
errorbar(wavelengths,test_avg,test_avg_std)
legend('ref','test')
title('Averages of the India Ink (reference) and IRDye 800 (test) measurements')
xlabel('Wavelength [nm]')
ylabel('Absorption [a.u.]')



%% India Ink spectrophotometer data
baseline = importdata('baseline.txt');
baseline_data = baseline.data;
y_baseline = baseline_data(:,2);

Measure1 = importdata('indiankink_mua_0.59_1.txt');
Measure1_data = Measure1.data;
y_Measure1 = Measure1_data(:,2) - y_baseline;

Measure2 = importdata('indiankink_mua_0.59_2.txt');
Measure2_data = Measure2.data;
y_Measure2 = Measure2_data(:,2) - y_baseline;


y_Measure = (y_Measure1+y_Measure2)/2;              % Average India Ink absorption value ( _a  = 0.59 mm^-1 @ 800nm) of two
    measurements
y_Measure_std = std([y_Measure1 y_Measure2]');      % Average India Ink absorption standarddeviation ( _a  = 0.59 mm^-1 @ 800
    nm) of two measurements
spec_ref = y_Measure(261:10:731);                   % Making it the same dimension of the PA signal
spec_ref_std = y_Measure_std(261:10:731)';          % Making it the same dimension of the PA signal



%% spectrophotometer reference data and compensation arrays
spec_ref_mu = log(10.^spec_ref)./10;                    % spectrophotometer reference data in mu_a
spec_ref_mu_std = log(10.^spec_ref_std)./10;

compensation =  spec_ref_mu./ref_avg';                  % Compensation value of average PA signal for each wavelength
std_compensation = spec_ref_mu_std./ref_avg_std';

% Plotting the correction scalars against the wavelength
figure()
errorbar(wavelengths,compensation,std_compensation)
xlabel('Wavelength [nm]')
ylabel('correction scalar')


% Plotting the specctrophotometer India absorbance & mu_a and the PA signal reference tube signal
figure()
errorbar(wavelengths(start:stop),spec_ref(start:stop),spec_ref_std(start:stop),'--s')
ylabel('Spectrophotometer absorbance [a.u.]')
hold on
errorbar(wavelengths(start:stop),spec_ref_mu(start:stop),spec_ref_mu_std(start:stop),'--s')
ylabel('Spectrophotometer Absorbance [a.u.] & \mu_a [mm^{-1}]')
yyaxis right
errorbar(wavelengths(start:stop),ref_avg(start:stop),ref_avg_std(start:stop),'--s')
legend('India Ink (spectrophotometer, Absorbance [a.u.])','India Ink (spectrophotometer, \mu_a [mm^{-1}])','India Ink (PA
    signal, not compensated)')
xlabel('Wavelength [nm]')
ylabel('PA signal [a.u.]')



%% Compensating the test tube data
test_compensated = test_avg'.*compensation;                                     % The compensation
fit_test_compensated_poly = fit(wavelengths',test_compensated,'poly9');         % Polyfit of the compensation
fit_test_compensated_fourier = fit(wavelengths',test_compensated,'fourier8');   % Fourier fit of the compensation

std_test_compensated = test_avg_std'.*std_compensation;

% Plotting the results
figure()
errorbar(wavelengths(start:stop),test_avg(start:stop),test_avg_std(start:stop),'--s','Color','k')
ylabel('PA signal [a.u.]')
hold on
ax = gca;
ax.YColor = 'r';
yyaxis right
errorbar(wavelengths(start:stop),test_compensated(start:stop),std_test_compensated(start:stop),'--s','LineWidth',2,'Color','#
    FF0000')
hold on
fitavg = plot(fit_test_compensated_fourier);
ax.YColor = '#FF0000';
set(fitavg,'Color','g')
legend('Average IRDye 800 signal (not compensated)','Average IRDye 800 signal (compensated)','Fourierfit of compensated
    signal')
xlabel('Wavelength [nm]')
ylabel('\mu_a [mm^{-1}]')


results_final.Wavelengths = wavelengths;
```

```
results_final.corrected_IRDye = test_compensated;
results_final.corrected_IRDye_std = std_test_compensated;
results_final.corrected_IRDye_fit = fit_test_compensated_fourier;

% Saving the results inside a .mat corresponding to the analysed condition
finalfileName = 'Final_results_concentration_' + concentration + '_depth' + depth + '.mat';
save(finalfileName, 'results');
```